

GRID HOMOLOGY FOR SINGULAR LINKS IN LENS SPACE AND A RESOLUTION CUBE

YONGHAN XIAO

Abstract

In this paper, we define grid homology for singular links in lens spaces and use it to construct a resolution cube for knot Floer homology of regular links in lens spaces. The results will first be proven over $\mathbb{Z}/2\mathbb{Z}$ and then extended to be over \mathbb{Z} via a sign assignment.

CONTENTS

1. Introduction	2
2. Singular link and grid diagram	4
2.1. Definitions	4
2.2. Construction of grid diagrams	7
2.3. Moves on torus diagram	9
2.4. Moves on grid diagram	13
3. Grid homology for singular links in lens spaces	18
3.1. Construction of chain complex	18
3.2. Gradings	19
3.3. Definition of homology theories	21
3.4. Computing examples	23
3.5. Proof of invariance	24
4. Resolution cube	31
4.1. Resolution of crossings	32
4.2. Skein exact sequence	34
4.3. Remarks on gradings	38
4.4. Resolution cube and spectral sequence	39
5. An oriented version	43
5.1. Sign assignment	43
5.2. Invariance of oriented theory	44
5.3. Oriented resolution cube	46
References	49

1. INTRODUCTION

After Heegaard Floer homology was defined in [23] and [22], knot Floer homology was introduced by Ozsváth and Szabó in [21], and also independently by Rasmussen in [28]. In [19], Ozsváth, Stipsicz and Szabó generalized knot Floer homology to singular knots in S^3 . Later, they used this to construct a resolution cube with twisted coefficients for knot Floer homology over $\mathbb{Z}/2\mathbb{Z}$ ([25]). Afterward, Manolescu proved an untwisted version over $\mathbb{Z}/2\mathbb{Z}$ ([16]). Recently, Beliakova, Putyra, Robert, and Wagner proved the corresponding result over \mathbb{Z} in Section 4 and 5 of [4]. With the help of this, Dowlin constructed a spectral sequence from Khovanov homology to knot Floer homology (See [8]).

On the other hand, in [29], Sucharit Sarkar and Jiajun Wang pointed out a criterion that ensures the count of holomorphic disks is combinatorial. A combinatorial version of knot Floer homology (so-called grid homology) first appeared in [17]. Later, Manolescu, Ozsváth, Szabó, and Thurston generalized the construction to links and extended the base ring to \mathbb{Z} via a sign assignment (See [18],[11]). The book *Grid homology for knots and links* ([26]) gives a detailed and complete description of this theory. Lens spaces are defined as rational surgeries on the unknot in S^3 , i.e. $L(p, q) = S^3_{p/q}(U)$. They are the simplest manifolds in terms of Heegaard decomposition other than S^3 . In [2], Baker, Grigsby and Hedden constructed grid diagrams for knots and links in lens spaces and proved that the combinatorially defined theory coincides with the existing one. In [6], Celoria constructed a sign assignment for grid diagrams of lens space links, and then the invariance of this oriented theory was proved by Tripp in [30]. In [12], Harvey and O'Donnol also considered grid homology for spatial graphs in S^3 (Bao also considered Heegaard Floer homology for bipartite graphs in [3]).

In this paper, we generalize previous constructions to singular links in lens spaces in a combinatorial way. Specifically, we will

- First, define three versions of grid homology for singular links in lens spaces and prove that they are well-defined invariants;
- Then, construct skein exact sequence and resolution cube for grid homology of lens space links;
- Finally, extend the base ring of our theory from $\mathbb{Z}/2\mathbb{Z}$ to \mathbb{Z} via an appropriate choice of sign assignment.

There were two interpretations of singular links in previous works. Some refer to immersions of disjoint union of S^1 's with transverse double points as singular links (e.g.[1]), while others refer to embeddings of certain kinds of graphs as singular links. We take the second approach following [19] and define a singular link in a 3-manifold Y as an embedding of a special oriented trivalent graph (See **Definition 2.2 and 2.3**).

In [25], they defined grid diagrams for singular links in S^3 by introducing XX base points to a regular diagram. (Also, in [12], they introduced nonstandard O base points for the same purpose.) Using their strategy, we define a grid diagram for singular links in lens spaces to consist of iterated pairs of α and β curves from standard Heegaard splitting of $L(p, q)$ as background rulings (following [2]) and O,X,XX three kinds of base points that record the information of the link. For details, see **Definition 2.5**.

After giving a precise definition of a grid diagram for a singular link, we show that each link admits such a diagram by direct construction. Then, we show Reidemeister's theorem for torus diagram of singular links (a generic projection to Heegaard torus) and prove that two grid diagrams represent the same singular link if and only if they can be connected by a sequence of grid moves.

Theorem 1.1. *Consider L and L' being singular links in $L(p, q)$ with the same underlying graph, the following are equivalent:*

- (1) L and L' are equivalent;
- (2) L and L' differ by a finite sequence of disk moves (**Definition 2.10**);
- (3) Regular projection (**Definition 2.9**) of L and L' to the Heegaard torus differ by a finite sequence of singular Reidemeister moves shown in **Figure 9**.

Theorem 1.2. *If two grid diagrams g and g' represent the same singular link L , then they can be connected by a finite sequence of commutation and (de)stabilization.*

See **Subsection 2.3, 2.4** for details on these moves.

With diagrams in hand, we follow the usual procedure in defining Heegaard Floer homology: form the symmetric product of the Heegaard surface with multiplicity according to its size, use intersection points between real tori formed by α and β curves as generators, and define differentials by counting empty rectangles. We will consider three kinds of chain complexes: CFK^- , \widehat{CFK} and \widetilde{CFK} and prove the following theorem in **Section 3.5**.

Theorem 1.3. *Fix a singular link L in some lens space $L(p, q)$ with n thick edges and m regular components. If g_1, g_2 are grid diagrams for $(L(p, q), L)$, then we have quasi-isomorphisms*

- $CFK^-(g_1) \simeq CFK^-(g_2)$;
- $\widehat{CFK}(g_1) \simeq \widehat{CFK}(g_2)$,

as relatively bigraded chain complexes of modules over polynomial ring $\mathbb{F}[U_1, \dots, U_{2n+m}]$ and over \mathbb{F} respectively. In particular, we have well-defined homology theories for singular links in lens spaces:

- Unblocked grid homology: $HFK^-(L)$ as relatively bigraded modules over $\mathbb{F}[U_1, \dots, U_{2n+m}]$ and
- Simply block grid homology: $\widehat{HFK}(L)$ as relatively bigraded modules over \mathbb{F} .

Here $\mathbb{F} = \mathbb{Z}/2\mathbb{Z}$ or \mathbb{Z} .

Having defined grid homology for singular links in lens spaces, we consider a resolution cube for grid homology of links in lens spaces, i.e. generalize the result in [25] via a purely combinatorial approach. We will introduce the notion of a special grid diagram (**Definition 4.2**) in which we fix a way of visualizing a link on a grid diagram such that each crossing looks like one of the standard pictures shown in **Figure 20**. Using such a diagram, we do resolution of crossings (see **Figure 19**) diagrammatically and prove a skein exact sequence.

Theorem 1.4. *Consider a special diagram g for a pair $(L(p, q), L)$. Choose a crossing c in g . Denote the resulting grid diagram (using the procedure in **Figure 21**) for smoothing and singularization at c by g_r, g_s and call the corresponding links L_r and L_s , respectively. Let O_a, O_b be marks sharing the same column with the newly formed XX base point, O_c, O_d be marks sharing the same row with the newly formed XX base point. Then we have the following:*

- When c is positive, there is an exact sequence:

$$(1) \quad \dots \longrightarrow \mathrm{HFK}^-(L) \longrightarrow H_*\left(\frac{\mathrm{CFK}^-(L_s)}{U_a + U_b - U_c - U_d}\right) \longrightarrow \mathrm{HFK}^-(L_r) \longrightarrow \mathrm{HFK}^-(L) \longrightarrow \dots$$

- When c is negative, there is an exact sequence:

$$(2) \quad \dots \longrightarrow \mathrm{HFK}^-(L) \longrightarrow \mathrm{HFK}^-(L_r) \longrightarrow H_*\left(\frac{\mathrm{CFK}^-(L_s)}{U_a + U_b - U_c - U_d}\right) \longrightarrow \mathrm{HFK}^-(L) \longrightarrow \dots$$

By considering resolutions of all crossings in a diagram, we can form a resolution cube. Using the skein relations and a direct computation of higher differentials, we show the following.

Theorem 1.5. *Let g be a special grid diagram for some possibly singular link L in $L(p, q)$. Assume at each crossing, g looks like the standard picture in **Figure 20**. Then there is a spectral sequence converging to $\mathrm{HFK}^-(g)$ whose E_1 term is the resolution cube with d_1 induced by some homomorphism from the skein exact sequence.*

We will also consider all these theories over \mathbb{Z} via a sign assignment for lens space grid diagrams constructed in [6]. After describing how to assign a sign to each rectangle in a grid diagram, we will reprove all the results over \mathbb{Z} . Using the universal coefficient theorem, this construction allows us to consider grid homology over any base field. In particular, one can use \mathbb{Q} as the base ring so that we can relate our theory to existing constructions that are only defined over rational numbers.

The paper is organized as follows: In **Section 2**, we first define singular links and construct grid diagrams for them; then we show Reidemeister theorem for torus projections and introduce a complete set of grid moves. In **Subsection 3.1-3.3**, we define the homology theories and introduce two grading systems on them. In **Subsection 3.4**, we compute fully blocked and simply blocked grid homology for some singular knots in $L(2, 1)$ and $L(3, 1)$. In **Subsection 3.5**, we demonstrate grid move invariance of our theories, which shows that they are well-defined link invariants. In **Section 4**, we first introduce resolutions of a crossing and then prove the existence of the skein exact sequence and the resolution cube mentioned above. Finally, we extend all the results to have base ring \mathbb{Z} in **Section 5**.

Acknowledgement

First of all, the author would like to thank her advisor Prof. Jiajun Wang for his detailed instruction and also Prof. Yi Ni for his helpful advice and encouragement. Secondly, the author thanks Hongjian Yang, Yicheng Yang for their helpful discussion. She would also express sincere gratitude to Prof. Jianfeng Lin and Prof. Yi Xie, who exposed her to grid homology and Dowlin spectral sequence, respectively, both of which motivate this work. Last but not least, the author appreciates Qing Lan, Quan Shi and Jinyi Wang for their assistance with computer programming and her family members for their unconditional support.

2. SINGULAR LINK AND GRID DIAGRAM

2.1. Definitions.

Definition 2.1. *An oriented trivalent graph consisting of vertices and thick/thin edges is special if*

- *at each vertex, there is exactly one thick and two thin edges.*

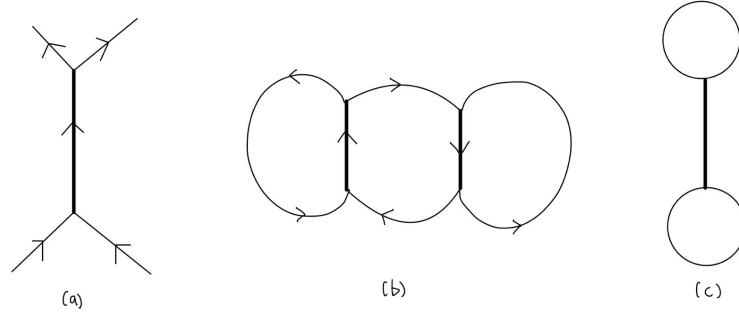


FIGURE 1. **Examples and a non-example of special trivalent graph.** (a) orientation at each thick edge; (b) an example of special trivalent graph; (c) non-orientable example

- the orientation satisfies that at each vertex, either the thick edge points in and the two thin edges point out or the thick edge points out while the two thin edges point in.

Here we do not require the graph to be connected, and closed components with a single thin circle and no vertex are allowed. (We will call such “circles” regular S^1 components and we require these to be oriented if exist.)

Note that not every trivalent graph with thick edges can be endowed with an orientation so that it becomes special, we only take oriented ones into our consideration. See **Figure 1** for examples and non-examples.

Definition 2.2. A singular link L inside a 3-manifold Y is a (piecewise linear) embedding of a special trivalent graph into Y .

For further use, we give an alternative definition of singular link as transverse spatial graph following [12]. Let \mathcal{D} be the disk endowed with a triangulation as shown in **Figure 2** which has four vertices, six edges and three 2-simplices. There is a unique vertex v_0 lie in the interior of \mathcal{D} . In this case, we say that \mathcal{D} is a standard disk and v_0 is the vertex associated to \mathcal{D} .

Take any oriented graph G_0 , we construct an oriented disk graph G associated to G_0 as follows. For each vertex v of G_0 , glue a standard disk \mathcal{D} to G_0 by identifying the vertex associated to \mathcal{D} to v . In this case, we say G_0 is the underlying oriented graph of G , since it appears naturally as part of the 1-skeleton of G . A vertex(edge) of G_0 will be called a graph vertex(edge). Here we allow G_0 to have closed components, each consisting of a single circle and no vertex. Again, such circles will be referred to as regular S^1 components and no disk is glued to them when forming the associated disk graph.

Definition 2.3. A singular link in a 3-manifold Y is a transverse embedding of a 4-valent oriented disk graph with exactly two graph edges going out and two graph edges pointing in at each graph vertex. Here the transverse embedding means that at each graph vertex, the local picture must look

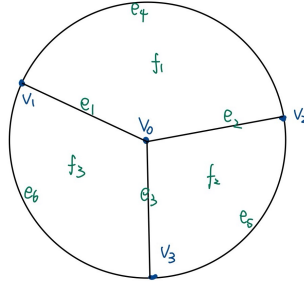


FIGURE 2. A standard disk with its triangulation

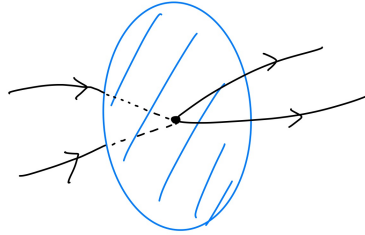


FIGURE 3. A transverse disk that separates incoming and outgoing edge

like **Figure 3**: the vertex has a closed B^3 neighborhood in Y such that its standard disk embeds properly in this copy of B^3 and separates the incoming and outgoing edges.

In this second definition, though we are embedding a 2-dimensional object into Y , we will regard the underlying oriented graph as a singular link L and remember the standard disks as auxiliary information that add restrictions to the isotopies allowed.

To see the definitions are equivalent, we consider the following operations: First, assume we are in **Definition 2.2**. For each thick edge, take a small disk centered at the middle point of the thick edge, being perpendicular to it and disjoint from all other edges or S^1 components. Then contract the thick edges to its middle point, we obtain the picture in the second definition. Going backward, we replace each graph vertex by a thick edge together with two new vertices, so that the thick edge meets the disk transversely at its center. The thick edge admits a unique orientation that fits the new graph into **Definition 2.1**. See **Figure 4** for an illustration. We remark that a special trivalent graph can also be regarded as a bipartite graph defined in [3].

We say a singular link is a singular knot if the underlying graph is connected.

Definition 2.4. Fix a special trivalent graph or oriented disk graph L , we say two singular links $i_1 : L \rightarrow Y$ and $i_2 : L \rightarrow Y$ are equivalent if there exists a piecewise linear homeomorphism $f : Y \rightarrow Y$ isotopic to the identity such that $i_1 \circ f = i_2$.

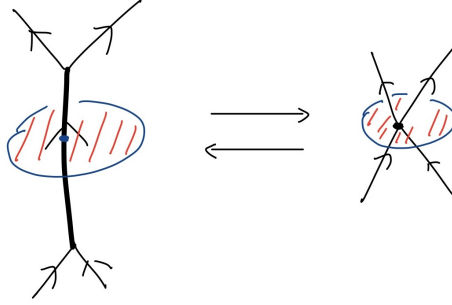


FIGURE 4. **Transform between two definitions of singular links.** By doing local moves at each vertex, we can transit between thick edge convention(left) and transverse graph convention(right).

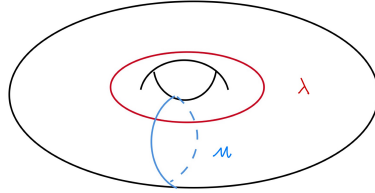


FIGURE 5. **Meridian and longitude on a Heegaard torus**

In what follows, we always take $Y = L(p, q)$ for a pair of integer p, q satisfying $gcd(p, q) = 1$ and $-p < q < p$.

2.2. Construction of grid diagrams. Let L be a (possibly) singular link with n thick edges in some lens space $L(p, q)$. We can assume without loss of generality that $gcd(p, q) = 1$ and $-p < q < p$. Our goal in this subsection is to define and construct grid diagrams for such pairs $(L(p, q), L)$

Grid diagram currently exists for possibly singular links in S^3 and regular links in $L(p, q)$, see [17],[2] and [1]. In [12], they also defined grid diagrams for transverse spatial graphs in S^3 . We shall show it also exists for singular links in $L(p, q)$.

Consider the standard Heegaard splitting of $L(p, q)$ into two genus one handlebodies: $L(p, q) = V_\beta \cup_\Sigma V_\alpha$. Here $\Sigma = T^2$ is a genus one closed surface. We choose a pair of curves μ, λ on it that are smooth generic representatives of a symplectic basis of its first homology. See **Figure 5**. A curve on Σ is said to have slope $\frac{p}{q}$ if it is homologous to $p\mu + q\lambda$.

In this terminology, the standard Heegaard splitting of $L(p, q)$ is given by a β curve with slope $-\frac{p}{q}$ and an α curve with slope 0. See **Figure 6** for $L(2, 1) = RP^3$ as an example.

From now on, we fix the convention that in a grid diagram, α curves will be red, β curves will be blue.

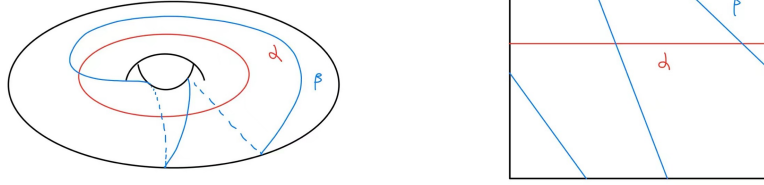


FIGURE 6. **Standard Heegaard splitting for RP^3 .** Left is the torus picture, right is the one after cutting open along a pair of meridian and longitude.

Definition 2.5. A grid diagram is a multi-based Heegaard diagram $(T^2, \alpha, \beta, \mathbb{O}, \mathbb{X})$ of $L(p, q)$ as follows:

- The background rulings are given by same number of parallel copies of β and α curves. In such a diagram, an annulus cut out by adjacent parallel α (β) circles is called a row(column). α and β will denote the set of α and β curves respectively. A connected component in $\Sigma - \alpha - \beta$ will be referred to as a cell.
- The base points are put in cells so that each cell has at most one base point. Each row or column is either singular or regular in the following sense:
 - In a regular row or column, we have one pair of O, X base points;
 - In a singular row or column, we have one XX base point together with two O base points.

It follows from the definition that in a grid diagram, we have same number of O, X base points (with XX base points counting twice) and same number of rows and columns.

Each grid diagram g can be associated with a unique singular link L . That is, we can reconstruct a torus projection (See **Definition 2.6**) of L and recover the embedding of L in $L(p, q)$ from g as follows.

- (1) Connect each O base point to the X or XX base points in the same row.
- (2) Connect each $X(XX)$ base point to the single (or two) O base point in the same column.

Here we follow the rule that horizontal segments always go under those slanted(vertical) ones.

Note that each XX base point plays the role of two regular X base points, i.e. there are two segments pointing to it and two segments going out from it.

Definition 2.6. Now we have a link diagram living on the Heegaard surface, it can be regarded as the projection of L to Σ using the Morse flow of a generic Morse function compatible with the standard Heegaard splitting. We call this picture a torus projection of L .

By further pushing the horizontal segments into V_α and those slanted ones into V_β , we recover the singular link L in $L(p, q)$.

In this case, we say g is a grid diagram for the pair $(L(p, q), L)$.

Proposition 2.7. Every singular link in a lens space $L(p, q)$ admits a grid diagram.

The proposition will be proved by direct construction.

In what follows, we fix identifications of V_α and V_β with $S^1 \times D^2$, so that we can talk about meridian disks without ambiguity. We temporarily focus on **Definition 2.2** of singular links.

Definition 2.8. *A singular link L in lens space $L(p, q)$ is called in grid position if*

- (1) *All vertices lie on Σ ;*
- (2) *Each thin edge or S^1 component of L meets Σ transversely in $n \geq 1$ times in its interior so that it is composed of finitely many arcs with ends on Σ . Each arc is required to be properly embedded in a meridian disks $\{pt\} \times D^2$ of V_β or V_α . As we travel along the edge, arcs in V_α and V_β appear alternately.*
- (3) *Interior of each thick edge lies entirely in a meridian disk of V_α or V_β .*
- (4) *When two thin arcs meet at a vertex, we require them to share a meridian disk which contains no other arcs. Also, if a thick edge has interior in V_α (V_β), then the four relevant thin arcs all lie in V_β (V_α).*
- (5) *Besides the case in (4), no two arcs share a meridian disk.*
- (6) *Each thick edge is short enough so that the two meridian disks containing arcs from its two vertices are adjacent in V_β or V_α . Here adjacent means that if the disk containing some arcs from L in V_γ ($\gamma = \alpha, \beta$) are $\{a_j\} \times D^2$, for $0 \leq a_1 < \dots < a_k < 1$ (parametrize S^1 by $[0, 1)$), then the two disks are $\{a_i\} \times D^2$ and $\{a_{i+1}\} \times D^2$ for some i or $\{a_1\} \times D^2$ and $\{a_k\} \times D^2$.*

After an isotopy, it is clear that any link in $L(p, q)$ can be put into grid position. So we assume L is already in such a position. Cut Σ open along a pair of generic λ and μ curves (generic in the sense that they meet the projection of L to Σ transversely). Here we cut Σ open for the convenience of drawing a planar diagram. Readers should keep in mind that the projection of L lives naturally on the Heegaard torus.

Then we rule the planar diagram with slanted β curves and horizontal α curves so that each row contains exactly one meridian disk of V_α which has one or two arcs from L and each column contains exactly one meridian disk of V_β which has one or two arcs from L . The case of two only happens near a vertex.

Afterwards, we put base points on the cut-open Σ . We put an O marks in a cell if there is an arc in V_α leaving it or an arc in V_β pointing to it. Similarly, a X mark is put in a cell if there is an arc in V_β leaving it or an arc in V_α pointing to it.

Now, in each row or column, we have two or three marks and at least one of a kind. For the shadow of each thick edge, we would have some consequent columns or rows with three marks and pair of O, X in adjacent cells. Add a thick arc connecting this pair of marked points. See (a) in **Figure 7** for example.

To change this into a desired picture, we introduce XX base points. See **Figure 7**, in which we show how to modify the picture in hand locally into a grid diagram.

In **Figure 8**, we give a detailed example illustrating the procedure from a singular link in grid position to a grid diagram using a singular knot with one thick edge in RP^3 .

2.3. Moves on torus diagram. In order to define an invariant of singular links based on those grid diagrams constructed above. We need to know how different grid diagrams of the same isotopic class

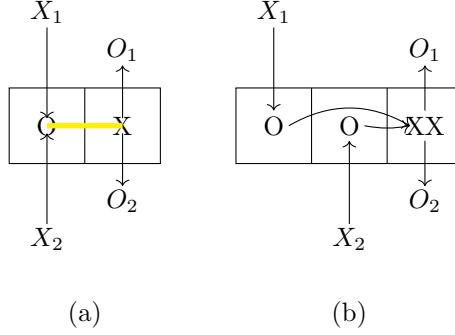


FIGURE 7. **Making a grid position projection into a grid diagram.** In (a), we show how the projection of a link in grid position looks like in a neighborhood of thick edge. Now add one column and one O marks to the diagram and dispense X_1 and X_2 to the column of two O base point in an arbitrary way. Then change X mark to XX, we get to (b) which is a desired way of exhibiting a thick edge in grid diagram

of links are related. Since our grid diagram is constructed based on a projection to the Heegaard torus, we first show an analogue of classical Reidemeister theorem (for planar diagram of knots in S^3). Here our proof modifies the proof of usual Reidemeister theorem in the appendix of [14].

Since a singular link is defined as an embedding of certain kind of graph, it is naturally an object in the piecewise linear category. So we will live in this category throughout this section and always endow L with a simplicial structure which is a subdivision of the natural one on a graph. When using **Definition 2.3**, a singular link L will mean the image of G_0 although those standard disks are important for us to consider what kinds of isotopy are allowed.

We first introduce some concepts that are necessary for describing a Reidemeister theorem.

Definition 2.9. *Recall that we are considering the projection of a singular link L to Heegaard torus T^2 induced by the flow of a generic Morse function which is compatible with the standard Heegaard splitting of lens spaces. Perturb it a little, we may assume the projection map is piecewise linear. Such a projection is called regular if*

- *The set of multiple points in the image $p(L)$ consists of finitely many double points.*
- *No points in the preimage $p^{-1}(c) \cap L$ of any double point $c \in p(L)$ is a vertex of L .*

Definition 2.10. *For a link L and an embedded disk D in $L(p, q)$ satisfying $L \cap D = L \cap \partial D$ which is an arc, we can form a new link $L' = cl(L - L \cap D) \cup (\partial D - L \cap D)$. In this case, we say L' is obtained from L by performing a disk move. It is clear that such a pair of links are equivalent.*

By subdividing L and D , we can assume the arc $\partial D \cap L$ is a union of 1-simplices while D is a union of 2-simplices. Thus, disk moves can be done in piecewise linear category.

The set of Reidemeister moves for torus diagrams of singular links in lens spaces is shown in **Figure 9** following those defined for spatial graphs in [13]. The first three moves are the usual ones, while IV and V account for newly introduced vertices. Due to definition difference comparing with

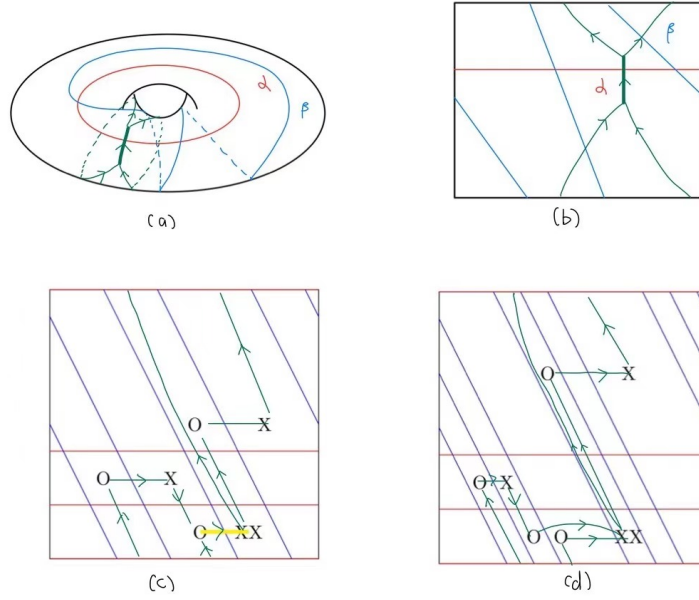


FIGURE 8. **An example of grid diagram** (a) a torus projection of a singular knot with one thick edge in RP^3 ; (b) the planar diagram of the same knot after cutting the torus open along a pair of meridian and longitude; (c) a new projection after putting the knot into grid position; we add new α and β curves according to how many meridian disks the knot intersects; (d) modify (c) using the procedure in **Figure 7** to get a grid diagram.

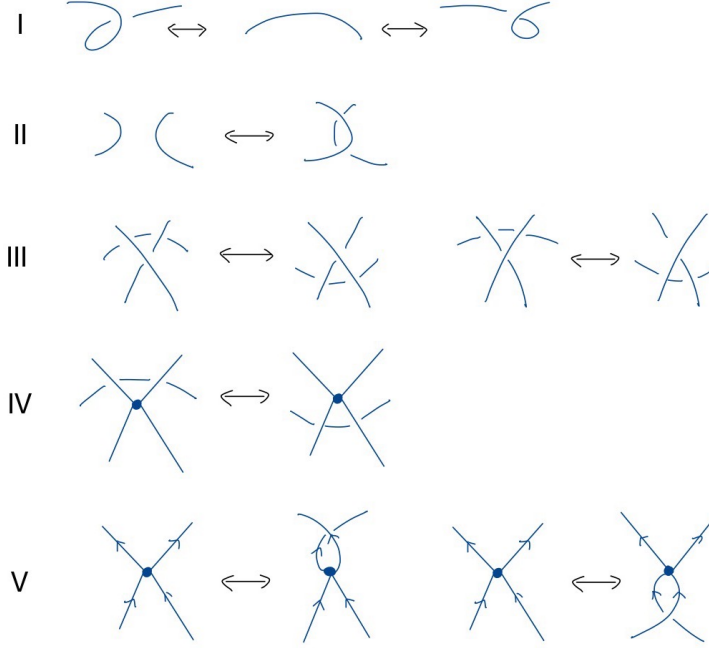
Kauffman’s setup, here Reidemeister move V can only happen between edges with same orientation at a vertex.

Theorem 2.11. *Consider L and L' being singular links in $L(p, q)$ with the same underlying graph, the following are equivalent:*

- (1) L and L' are equivalent;
- (2) L and L' differ by a finite sequence of disk moves;
- (3) regular projections of L and L' to the Heegaard torus differ by a finite sequence of singular Reidemeister moves.

Proof. (3) implies (1) is clear.

We now show (1) implies (2). Take h to be the piecewise linear homeomorphism in the definition of equivalence. Note that any automorphism of $L(p, q)$ that is isotopic to the identity fixes the Heegaard torus T and two handlebodies up to isotopy. See [5] for detailed knowledge on the mapping class group of lens spaces. So without loss of generality, we assume that h sends T, V_β, V_α to themselves, respectively. Observe that L intersects V_α in finitely many arcs, so by pushing T a

FIGURE 9. **Singular Reidemeisters moves I-V**

little bit down into V_α using its collar neighborhood in V_α , we may assume L lies entirely in $\text{int}(V_\beta)$. Since $h(L) = L'$, $h(V_\beta) = V_\beta$, L' also lies in $\text{int}(V_\beta)$.

Let V_β be parametrized as $S^1 \times D^2$ in the usual way. Let $C = S^1 \times \{0\}$ be the core curve, D_ϵ be the subdisk of D^2 with radius ϵ and $V_\epsilon = S^1 \times D_\epsilon \subset V_\beta$. Further denote by $S = \partial V_\beta \cong T^2$.

We can further isotope L , L' and h so that

$$L \cap C = \emptyset = L' \cap C,$$

and h fix some $V_{\epsilon'}$ disjoint from L and L' for $\epsilon' > 0$ sufficiently small.

Before starting the proof, we make an important claim: If $V_{\epsilon'}$ is a solid torus disjoint from L , then there exists a singular link L^* in $V_{\epsilon'}$ which can be connected to L within a finite sequence of disk moves.

Choose ϵ_0 and ϵ with

$$0 < \epsilon_0 < \epsilon' < \epsilon < 1,$$

such that

$$V_{\epsilon_0} \subset \text{int}(V_{\epsilon'}) \subset L \cup V_{\epsilon'} \subset \text{int}(V_\epsilon).$$

Then we have an obvious homeomorphism

$$d : V_\epsilon - \text{int}(V_{\epsilon_0}) \rightarrow S \times [1, 3],$$

with $d(V_{\epsilon'} - \text{int}(V_{\epsilon_0})) = S \times [1, 2]$.

Denote by $p_S : S \times [1, 3] \rightarrow S$ and $p_I : S \times [1, 3] \rightarrow [1, 3]$ the projections. Further introduce compositions $e_S = p_S \circ d : V_\epsilon - \text{int}(V_{\epsilon_0}) \rightarrow S$, $e_I = p_I \circ d : V_\epsilon - \text{int}(V_{\epsilon_0}) \rightarrow [1, 3]$.

By further composing with an automorphism f of $S \times [1, 3]$ satisfying $f(S \times [1, 2]) = S \times [1, 2]$ if necessary, we may assume $e_S|_L$ is an immersion. Observe that $e_I(L) \subset (2, 3)$, so we have a well-defined map $F : L \times [0, 1] \rightarrow S \times [1, 3]$ defined by

$$F(x, t) = (e_S(x), e_I(x) - t).$$

This F is not piecewise linear, but it sends piecewise linear subspaces to piecewise linear subspaces. In particular, the restriction to each $L \times \{t\}$ is piecewise linear.

For each $t \in [0, 1]$, there is a closed neighborhood $N(t) \subset [0, 1]$, so that F is an embedding when restrict to $L \times N(t)$, thus $F(L \times N(t))$ is a piecewise linear submanifold of $S \times [1, 3]$. Using this and the compactness of $[0, 1]$, we get a finite sequence of ‘time level’ $0 = t_0 < t_1 \dots < t_n = 1$ such that each $F(L \times \{t_i\})$ can be connected to $F(L \times \{t_{i+1}\})$ using finitely many disk moves. Take $L^* = F(L \times \{1\})$, then we have shown our claim.

Now we go back and pick up our homeomorphism h . We have assumed that h fix some $V_{\epsilon'}$ disjoint from L and L' , take $L^* \subset V_{\epsilon'}$ obtained from the claim above. Now L^* can be related to L by a finite sequence of disk moves. Applying h , we see that $h(L^*) = L^*$ can be connected to $h(L) = L'$ by a finite sequence of disk moves. Consequently, L and L' can be connected by a finite sequence of disk moves.

Finally, we show that (2) implies (3). It suffices to consider a pair of links L and L' that can be related by a single disk move. By subdividing the disks into triangles and refining the triangulation of T^2 and L , we only need to consider small triangles

- with at most one crossing in its interior or
- at most one graphical vertex (an original vertex in the transverse graph definition or equivalently a thick edge in the first definition) on its boundary or in its interior.

The first case has been dealt with in [27]. We only need to deal with the second one:

- See **Figure 10** for cases in which there is exactly one graphical vertex in the interior of the triangle. Our convention is that disk moves happen between the orange edges and the blue edge that together form the ‘‘disk’’-triangle. These can be realized by a single Reidemeister move IV or a composition of one or two Reidemeister move II together with a Reidemeister move IV. See **Figure 11** for an illustration.
- For the case that a graphical vertex appearing as a vertex of the triangle, see **Figure 12**. Each of these is just a singular Reidemeister move V.

After dealing with all these cases, we know (2) implies (3), so the three items are equivalent. \square

2.4. Moves on grid diagram. Now we are ready to introduce grid moves and show that they are enough for realizing all Reidemeister moves defined above. Once this is done, we can introduce invariants of singular links by considering invariants of grid diagrams that are kept unchanged under these moves.

For classical grid moves, there is a detailed description in Chapter 3 of [26]. Here we almost follow [12] except that our background grid diagrams are no longer formed by squares, and we are using

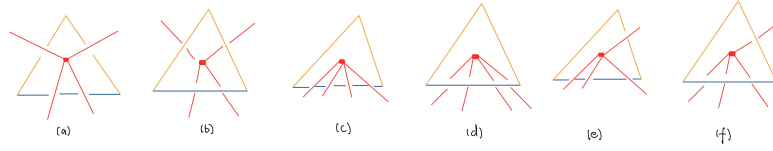


FIGURE 10. **Disk moves with a vertex in the disk interior.** In (a)-(f), we list all possible cases of a triangle of disk move containing exactly one vertex in its interior. In each case, the disk move transforms between the blue edge and the orange broken line. (a) and (b) can be realized by a Reidemeister move IV directly. In **Figure 11**, we show how to realize (c) and (e) by Reidemeister moves. (d) and (f) can be realized similarly.

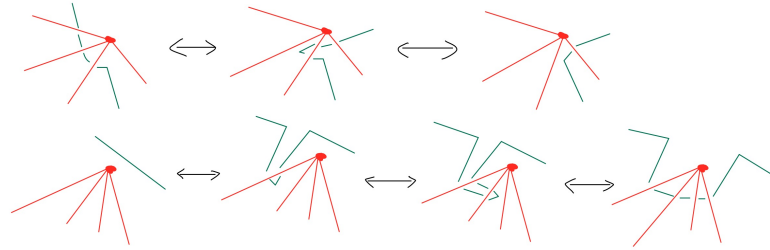


FIGURE 11. **Realize disk moves by Reidemeister moves.** In the first row, we show how to realize **Figure 10(e)** by Reidemeister moves II and IV. In the second row, we show how to realize **Figure 10(c)** by Reidemeister move II and IV. We omit orientations in this list since orientations are irrelevant for these moves.

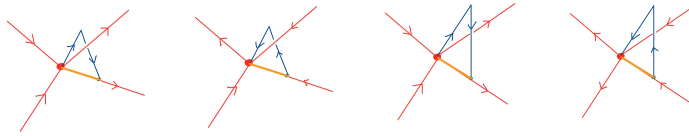


FIGURE 12. **Disk moves with a graphical vertex as a vertex of the triangle.** We list here all possible cases for a disk move to have a graphical vertex as a vertex of the triangle(disk). Each of these can be realized by a single Reidemeister move V.

a different labeling convention: our XX corresponds to their nonstandard O, our X corresponds to their regular O, while our O corresponds to their X.

To make the definitions below clear, we recall the convention stated in **Definition 2.5**: a column(row) is an annulus cut out by adjacent β (α) curves. We introduce three kinds of grid moves, naming them following the classical case:

- Cyclic permutation: permuting the columns or rows cyclically, this is the same as the classical case.
- Stabilization and destabilization: assume g is a grid diagram of size n , we stabilize g to obtain a diagram of size $n+1$. Choose any marked cell of g . Erase the mark in this cell as well as marks in the same row or column. Split the empty row and column into two rows and two columns. If the original mark is X or O , then there are exactly four ways to fill in the new rows and columns to get a grid diagram (See [26], in which they described them in terms of directions: South-East, South-West, North-East, or North-West). If the original mark is XX , then we must fill in the new rows and columns with one XX , one X and six O s. There are sixteen ways to do this to fit the new diagram into **Definition 2.5** without changing the link that it represents. Destabilization is defined as the inverse of a stabilization.
- Commutation: we describe using columns, the same applies to rows. A pair of adjacent columns can be exchanged if the followings are satisfied: there are slanted line segments LS_1 and LS_2 on the torus such that
 - (1) $LS_1 \cup LS_2$ contains all the XX , O and X base points in these two columns;
 - (2) the projection of $LS_1 \cup LS_2$ to a single curve β_i is β_i ;
 - (3) the projection of $\partial LS_1 \cup \partial LS_2$ consists of exactly two points.

In **Figure 13**, we show examples of grid moves.

One can see from these examples that grid moves are just reformulations of Reidemeister moves we considered in previous section, in particular, they keep the equivalence class of the link unchanged.

Remark 2.12. *There are extra moves introduced in [26], the so-called switch and cross commutation. In our definition, switches are contained in the set of commutation. As mentioned there, cross commutation leads to crossing change for planar knot diagram, so it does not preserve the isotopy type in general.*

*As mentioned in the survey paper [10], the way of connecting base points on the Heegaard diagram is not unique, leading to different torus projections of the same singular link. Such a move is called “disk slide” there. It has nothing to do with our grid homology, but we will fix a way of connecting base points when we construct resolution cubes in **Section 4**.*

Before proving the completeness of these moves, we introduce the concepts of L-formation and preferred diagram mimicking [12].

Definition 2.13. *For an XX mark, we call the set of O 's sharing the same row or column its flock. We say the flock of XX is in L-formation if they are immediately to the right or above XX . A preferred grid diagram is a grid diagram in which all XX 's have their flocks in L-formation.*

An example of such a diagram is shown in **Figure 14**. This is again a grid diagram of the knot we have considered in **Figure 8**.

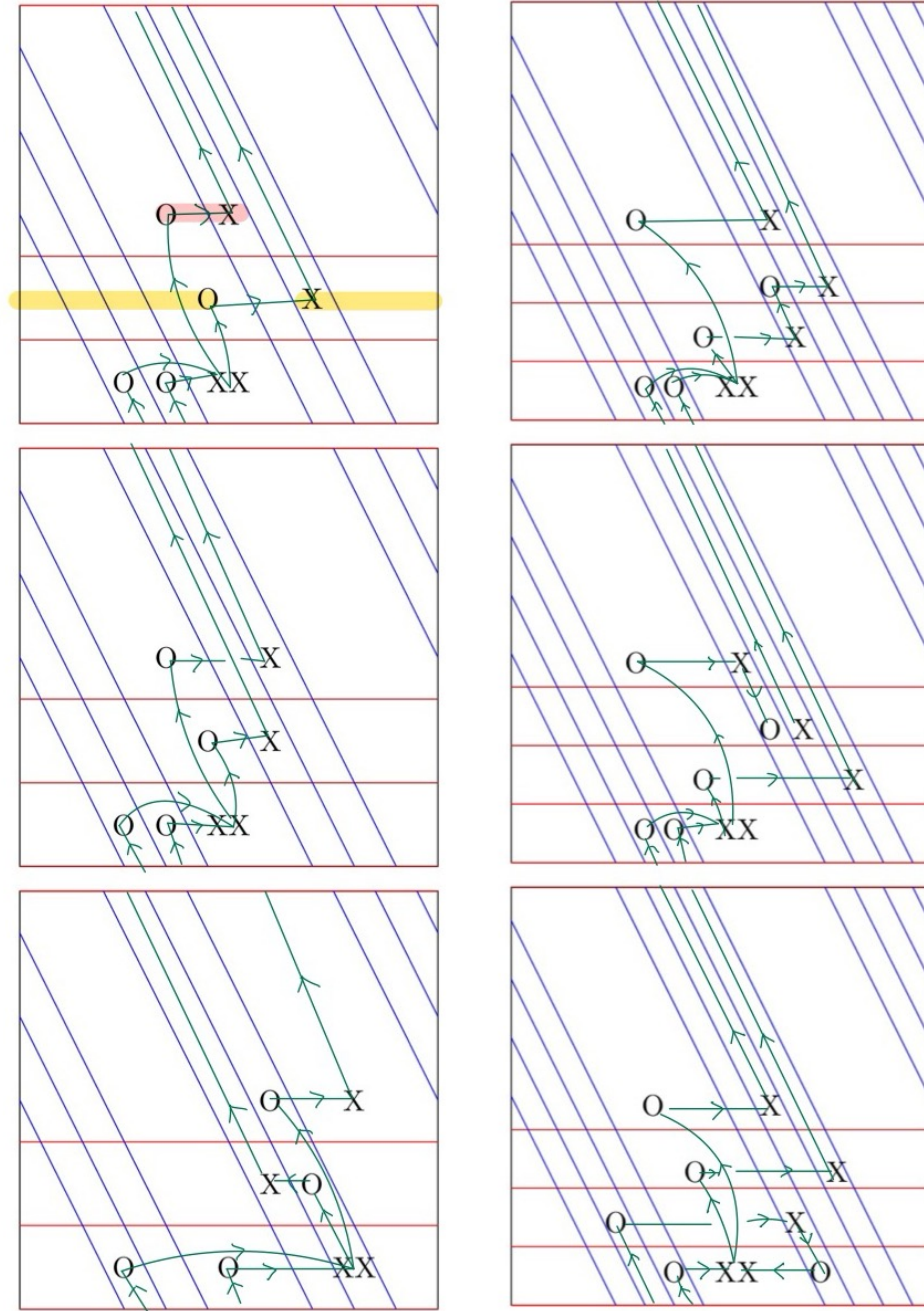


FIGURE 13. **Example of grid moves.** The top left picture is an alternative grid diagram for the singular knot we have seen in **Figure 8**, we shall apply various grid moves to this diagram. The red and yellow segments are LS_1 and LS_2 , respectively, showing that these two columns are available to be exchanged. In the middle left picture, we show the grid diagram after commutation. The lower left picture is the result of performing a cyclic permutation; the top right picture is resulting from a stabilization $O:NW$; the middle right picture is resulting from a stabilization $X:NE$; the lower right picture is resulting from a stabilization $XX:NW$.

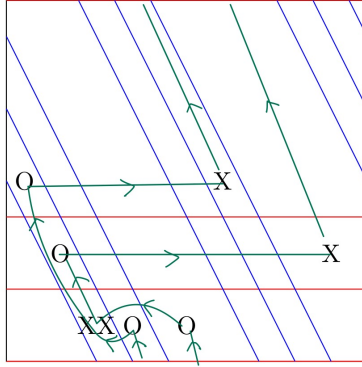


FIGURE 14. **Example of grid diagram in L-formation.**

The proof of the following in [12] directly extends to our case:

Lemma 2.14. *Every grid diagram of a singular link can be made into a preferred grid diagram using a finite sequence of grid moves.*

The proof of this lemma from [12] has been done in two steps:

- By doing stabilization, we separate the flocks so that no O is shared by a singular row and a singular column.
- By doing stabilization and commutation, we can put the flock of each XX into L-formation. With the help of the first step, this can be done without violating the L-formation of other XX 's. Thus, we can achieve our goal in finite steps.

Theorem 2.15. *If two grid diagrams g and g' represent the same singular link L , then they can be connected by a finite sequence of grid moves.*

The main idea of this proof is to verify that any planar isotopy and all Reidemeister moves can be realized by a finite sequence of grid moves. With the help of the previous lemma, we only need to consider the case that both g and g' are preferred. We find this verification has been done by previous works:

- For regular Reidemeister moves and isotopy of diagrams that do not involve any singular point, the proof has been done by [7] and [9]. For a detailed version one can refer to appendix of [26].
- For the singular Reidemeister moves and isotopy that involve vertices, a detailed proof has been done in [12]. The only difference is that our diagram is not a square but a parallelogram. Actually, we only need part of their proof: Since all of our vertices are 4-valent, only two kinds of isotopies need to be taken care of: a vertex passing through an arc and two vertices passing each other. See Figure 26,27,28 and 30,31 in [12].

Before ending this section, we quote a lemma from [26] that implies that it suffices to consider (de)stabilization and commutation invariance for the theory that we are going to define.

Lemma 2.16. *A cyclic permutation can be realized by a finite sequence of commutation, stabilization and destabilization.*

Although they proved this for grid diagrams of knots and links in S^3 , their proof applies to our case without change.

3. GRID HOMOLOGY FOR SINGULAR LINKS IN LENS SPACES

In this section, we always consider a grid diagram as follows unless otherwise stated. g is a grid diagram of size $n+k$ representing a singular link L in $L(p, q)$ with m regular components and n thick edges. That is, we have a diagram ruled by $n+k$ β and α circles with n XX marks, k X marks and $2n+k$ O marks. By renumbering the O -marks, we assume that O_1, \dots, O_{2n+m} lies on distinct thin edges or S^1 components. Note that n and m are intrinsic to the underlying graph while k depends on the embedding and the specified grid diagram.

For convenience, we introduce some new notations :

- O : the set of all O marks;
- XX : the set of all XX marks;
- X_r : the set of all X marks;
- $\text{X} = \text{XX} \cup \text{X}_r$.

3.1. Construction of chain complex. Form the symmetric product $\text{Sym}^{n+k}(T^2)$ which contains tori $\mathbb{T}_\alpha = \alpha_1 \times \dots \times \alpha_{n+k}$ and $\mathbb{T}_\beta = \beta_1 \times \dots \times \beta_{n+k}$. The set of intersection points $\mathbf{S} = \mathbb{T}_\alpha \cap \mathbb{T}_\beta$ will be the generating set of our chain complexes. For $\mathbf{x} \in \mathbf{S}$, we shall regard it as a point in $\text{Sym}^{n+k}(T^2)$, as well as a finite set of points in g . In our grid diagram, each pair of β and α curves has p intersection points between them. Consequently, we have $(n+k)! \cdot p^{n+k}$ generators in total.

Note that the grid diagram endows the torus with a natural cell-complex structure: It has $p \cdot (n+k)^2$ 0-cells, $2p \cdot (n+k)^2$ 1-cells and $p \cdot (n+k)^2$ 2-cells.

A domain from \mathbf{x} to \mathbf{y} is a 2-chain D with $\partial D \cap \alpha$ a path from \mathbf{x} to \mathbf{y} and $\partial D \cap \beta$ a path from \mathbf{y} to \mathbf{x} . We will use $\pi(\mathbf{x}, \mathbf{y})$ to denote the set of domains from \mathbf{x} to \mathbf{y} . When a domain from \mathbf{x} to \mathbf{y} is an embedded rectangle, it will be called a rectangle from \mathbf{x} to \mathbf{y} . A rectangle r from \mathbf{x} to \mathbf{y} is empty if $\text{int}(r) \cap \mathbf{x} = \emptyset = \text{int}(r) \cap \mathbf{y}$. Denote by $\text{Rect}(\mathbf{x}, \mathbf{y})$ the set of rectangles from \mathbf{x} to \mathbf{y} and by $\text{Rect}^\circ(\mathbf{x}, \mathbf{y})$ the set of empty rectangles from \mathbf{x} to \mathbf{y} . For a point p living in the interior of some 2-cell, denote by $n_p(D)$ the multiplicity of D at p . We will abuse the notation to $n_P(D)$ for P a finite set of points all living in interiors of 2-cells.

Definition 3.1. *We define three versions of chain groups and differentials: Here $\mathbb{F} = \mathbb{Z}/2\mathbb{Z}$.*

- *Unblocked version: the chain group $\text{CFK}^-(g)$ is generated by \mathbf{S} over $\mathbb{F}[U_1, \dots, U_{2n+k}]$, the differential counts empty rectangles:*

$$\partial^- \mathbf{x} = \sum_{\mathbf{y} \in \mathbf{S}} \sum_{\{r \in \text{Rect}^\circ(\mathbf{x}, \mathbf{y}) \mid n_{\mathbf{x}}(r) = 0\}} \prod_{i=1}^{2n+k} U_i^{n_{O_i}(r)} \mathbf{y};$$

- *Simply blocked version: $\widehat{\text{CFK}}(g) = \text{CFK}^-(g)/(U_1 = \dots, U_{m+2n} = 0)$;*

- *Fully blocked version:* $\widetilde{CFK}(g) = CFK^-(g)/(U_1 = \dots, U_{k+2n} = 0)$.

Alternatively, take \mathbb{F} as the base ring, so that $\widetilde{CFK}(g)$ is a finitely generated vector space over \mathbb{F} with \mathbf{S} as a basis. The differential counts empty rectangles without any marked points:

$$\tilde{\partial}\mathbf{x} = \sum_{\mathbf{y} \in \mathbf{S}} \sum_{\{r \in \text{Rect}^\circ(\mathbf{x}, \mathbf{y}) \mid n_{\mathbb{X}}(r) = 0, n_{\circ}(r) = 0\}} \mathbf{y}.$$

Remark 3.2. Although we use the notations “CFK” and “HFK” for our chain complexes and homology groups instead of “GC” and “GH”, we only take grid diagrams into consideration in our paper.

Using the standard complex structure on T^2 and with the help of Lipshitz formula ([15]), one sees that 1 is exactly the Maslov index of an empty rectangle, and empty rectangles are the only possible “disks” in a grid diagram with such Maslov index. So our grid homology can be regarded as a combinatorial generalization of Heegaard Floer theory to singular links in lens spaces.

To verify they are chain complexes, one can resort to analytic tools and consider broken flow lines. However, we can actually do this combinatorially. We illustrate this using minus version. Observe that for any $\mathbf{x} \in \mathbf{S}$,

$$\partial^- \circ \partial^-(\mathbf{x}) = \sum_{\mathbf{z} \in \mathbf{S}} \sum_{D \in \pi(\mathbf{x}, \mathbf{z})} N(D) \prod_{i=1}^{2n+k} U_i^{n_{\circ_i}(D)} \mathbf{z},$$

where $N(D)$ is the number of ways one can decompose D as union of empty rectangles that intersect \mathbb{X} emptily. That is how many ways we can express D as $D = r_1 * r_2$ for some $\mathbf{y} \in \mathbf{S}$, $r_1 \in \text{Rect}^\circ(\mathbf{x}, \mathbf{y})$, $r_2 \in \text{Rect}^\circ(\mathbf{y}, \mathbf{z})$ and $r_1 \cap \mathbb{X} = r_2 \cap \mathbb{X} = \emptyset$. Here we use $*$ to denote juxtaposition of domains on a grid diagram g . Note that if $\prod_{i=1}^{2n+k} U_i^{n_i} \mathbf{z}$ appears in $(\partial^-)^2 \mathbf{x}$, $\mathbf{x} - \mathbf{x} \cap \mathbf{z}$ can only consist of 0, 2, 3 or 4 points. The case of 1 can be ruled out by a direct geometric argument. Following [6], we denote the cardinality of this set by M . The case $M=0$ is easy: when $\mathbf{x} = \mathbf{z}$, D can only be a linear combination of thin annuli, which is not allowed since it contains an X or XX mark always. So terms like $\prod_{i=1}^{2n+k} U_i^{n_i} \mathbf{x}$ never appears in $(\partial^-)^2 \mathbf{x}$. For $M=3, 4$, the argument of Lemma 4.6.7 in [26] shows that $N(D) = 2$ whenever it is not zero. For $M=2$, it only appears when the lens space is not S^3 , for now each pair of α and β intersect more than once. A detailed analysis has been done in Proposition 2.11 of [6], which shows that $N(D)$ is again zero or two in this case. Thus we can conclude that $(\partial^-)^2 = 0$.

Remark 3.3. The proof of Proposition 2.11 in [6] (or Proposition 3.6 in [30]) together with that of Lemma 4.6.7 in [26] together give a complete analysis of $N(D)$ when D can be written as $r_1 * r_2$, a juxtaposition of empty rectangles. An important observation is that the number of decompositions has nothing to do with what marks the domain contains, so their result can be used to analyze the composition of any pair of rectangle counting maps. This will play an important role in the following sections.

3.2. Gradings. We will define two kinds of grading combinatorially on the chain complex. Instead of using flowlines and $Spin^c$ structure, this will be done by fitting the grid diagram into a suitable coordinate and defining a comparing function between tuples of points in the diagram. The idea of this construction comes from [2]. Modification has been done due to “singularities” according to [19].

We embed our grid diagram into \mathbb{R}^2 by declaring the α circles $\{\alpha_i\}_{i=0}^{n+k-1}$ to be line $y = \frac{i}{n+k}$, $0 \leq i \leq n+k-1$ and the β circles $\{\beta_i\}_{i=0}^{n+k-1}$ to be $y = -\frac{p}{q}(x - \frac{i}{p(n+k)})$. We shall take a preferred fundamental domain $0 \leq y < 1$, $-\frac{q}{p}y \leq x < -\frac{q}{p} + 1$. As above, we shall denote our grid diagram by g .

We first introduce some auxiliary functions: consider a set-valued function

$$W : \{\text{finite sets of points in } g\} \rightarrow \{\text{finite sets of pairs } (a, b) \text{ with } a \in [0, p(n+k)), b \in [0, n+k)\},$$

which assigns to each set of points in g the tuple of its \mathbb{R}^2 coordinate written with respect to the basis

$$\{\vec{v}_1 = (\frac{1}{p(n+k)}, 0), \vec{v}_2 = (-\frac{q}{p}, \frac{1}{n+k})\}.$$

We always assume X, O or XX marks live in the center of their cells, respectively. For $\mathbf{x} \in \mathbf{S}$, $W(\mathbf{x})$ is a set of integers while $W(\mathbb{O})$, $W(\mathbb{X}_r)$ and $W(\mathbb{X}\mathbb{X})$ are sets of half integers.

We also need another coordinate transformation function

$$\begin{aligned} C_{p,q} : \{\text{finite sets of pairs } (a, b) \text{ with } a \in [0, p(n+k)), b \in [0, n+k)\} \\ \rightarrow \{\text{finite sets of pairs } (a, b) \text{ with } a, b \in [0, (n+k)p)\}, \end{aligned}$$

sending a \mathbb{N} -tuple of coordinates

$$\{(a_i, b_i)\}_{i=0}^N$$

to a $p\mathbb{N}$ tuple of coordinates

$$\{((a_i + (n+k)ql) \bmod p(n+k), (b_i + (n+k)l) \bmod p(n+k))\}_{i=0, l=0}^{i=N, l=p-1}.$$

Now, let \tilde{W} be the composition $C_{p,q} \circ W$.

Further, we introduce a function \mathcal{I} (originally from [26]). It has input an ordered pair (A, B) each of which is a finite set of coordinate pairs. The output $\mathcal{I}(A, B)$ is the cardinality of pairs $(a_1, a_2) \in A$ and $(b_1, b_2) \in B$ with $a_i < b_i$, $i = 1, 2$. Also define $\mathcal{J}(A, B) = \frac{1}{2}(\mathcal{I}(A, B) + \mathcal{I}(B, A))$, which is the symmetrization of \mathcal{I} .

Now we define relative gradings between \mathbf{x} and \mathbf{y} when they can be connected by a sequence of not necessarily empty rectangles (For readers familiar with original Heegaard Floer theory, this is equivalent to that \mathbf{x} and \mathbf{y} come from same $Spin^c$ structure).

The relative Maslov grading is given by

$$\begin{aligned} (3) \quad M(\mathbf{x}, \mathbf{y}) &= M_{\mathbb{O}}(\mathbf{x}, \mathbf{y}) \\ (4) \quad &= \frac{1}{p}(\mathcal{J}(\tilde{W}(\mathbf{x}), \tilde{W}(\mathbf{x}) - \mathcal{J}(\tilde{W}(\mathbf{y}), \tilde{W}(\mathbf{y})) - 2\mathcal{J}(\tilde{W}(\mathbb{O} - \mathbb{X}\mathbb{X}), \tilde{W}(\mathbf{x} - \mathbf{y}))). \end{aligned}$$

Similarly, we define

$$(5) \quad M_{\mathbb{X}}(\mathbf{x}, \mathbf{y}) = \frac{1}{p}(\mathcal{J}(\tilde{W}(\mathbf{x}), \tilde{W}(\mathbf{x}) - \mathcal{J}(\tilde{W}(\mathbf{y}), \tilde{W}(\mathbf{y})) - 2\mathcal{J}(\tilde{W}(\mathbb{X}_r + \mathbb{X}\mathbb{X}), \tilde{W}(\mathbf{x} - \mathbf{y}))).$$

Then the relative Alexander grading is defined as

$$A(\mathbf{x}, \mathbf{y}) = \frac{1}{2}(M_{\mathbb{O}}(\mathbf{x}, \mathbf{y}) - M_{\mathbb{X}}(\mathbf{x}, \mathbf{y})).$$

We extend these gradings to the unblocked theory by letting

$$\begin{aligned} A(U_i \mathbf{x}, \mathbf{x}) &= -1, \\ M(U_i \mathbf{x}, \mathbf{x}) &= -2 \end{aligned}$$

for any $\mathbf{x} \in \mathcal{S}$ and $1 \leq i \leq 2n + k$.

We define a lift of these gradings to \mathbb{Q} following the convention in [2], in the sense that when our link has no singular point, our definition goes back to theirs. This is needed for us to compare gradings coming from different grid diagrams.

$$(6) \quad M(\mathbf{x}) = M_{\mathbb{O}}(\mathbf{x})$$

$$(7) \quad = \frac{1}{p}(\mathcal{J}(\tilde{W}(\mathbb{O} - \mathbb{X}\mathbb{X}) - \tilde{W}(\mathbf{x}), \tilde{W}(\mathbb{O} - \mathbb{X}\mathbb{X}) - \tilde{W}(\mathbf{x}))$$

$$(8) \quad + d(p, q, q - 1) + \frac{p - 1}{p},$$

$$(9) \quad M_{\mathbb{X}}(\mathbf{x}) = \frac{1}{p}(\mathcal{J}(\tilde{W}(\mathbb{X}_r + \mathbb{X}\mathbb{X}) - \tilde{W}(\mathbf{x}), \tilde{W}(\mathbb{X}_r + \mathbb{X}\mathbb{X}) - \tilde{W}(\mathbf{x}))$$

$$(10) \quad + d(p, q, q - 1) + \frac{p - 1}{p},$$

$$A(\mathbf{x}) = \frac{1}{2}(M_{\mathbb{O}}(\mathbf{x}) - M_{\mathbb{X}}(\mathbf{x}) - (n + k - 1)),$$

in which $d(p, q, i)$ is the correction term of $L(p, q)$ defined as in [20], using a canonical identification of $Spin^c(L(p, q))$ with $\mathbb{Z}/p\mathbb{Z}$.

Proposition 3.4. *In each of the three chain complexes $CFK^-(g)$, $\widehat{CFK}(g)$ and $\widetilde{CFK}(g)$, the differential preserves A and lowers M by 1.*

This can be shown exactly in the same way as Proposition 2.11 in [6]. This is an argument of lifting the diagram to one for a singular link in S^3 , which is what the function \tilde{W} does. We will give a detailed description of how to use lift to compute gradings in **Subsection 3.5**.

3.3. Definition of homology theories. We define three versions of homology for singular links using the three chain complexes defined in the previous two sections. We shall prove later that the first two are invariants for singular links in $L(p, q)$ while the third one is closely related to the second one in the sense we shall make precise in **Proposition 3.7**. Here we fix a singular link with m S^1 components and n thick edges as above and choose a grid diagram g for L of size $n + k$.

Definition 3.5. • *The unblocked grid homology is defined as*

$$HFK^-(L) = H_*((CFK^-(g), \partial^-)),$$

viewed as a $\mathbb{F}[U_1, \dots, U_{m+2n}]$ module.

• *The simply blocked grid homology is defined as*

$$\widehat{HFK}(L) = H_*((\widehat{CFK}(g), \widehat{\partial})),$$

viewed as a \mathbb{F} vector space, where $\widehat{\partial}$ is the differential inherited from ∂^- .

- The fully blocked grid homology is defined as

$$\widehat{HFK}(L) = H_*((\widehat{CFK}(g), \tilde{\partial})),$$

viewed as a \mathbb{F} vector space.

Each homology group is relatively bigraded by M and A defined above.

To show that $HFK^-(L)$ is well-defined as a $\mathbb{F}[U_1, \dots, U_{m+2n}]$ module and $\widehat{HFK}(L)$ is well-defined as a \mathbb{F} vector space, we need the following propositions.

Proposition 3.6. Consider any grid diagram g ,

- (1) If O_i and O_j belong to the same thin edge or the same S^1 component of the underlying graph, then the multiplication by U_i is chain homotopic to the multiplication by U_j .
- (2) For any singular point XX , let O_i, O_j be O -marks sharing the same row, O_s, O_l be marks sharing the same column, then the multiplication by $U_i U_j$ is chain homotopic to the multiplication by $U_s U_l$.

Proof. The first statement follows from Proposition 4.21 of [12] while the second follows from Proposition 1 in [31]. For readers' convenience, we also provide a self-contained proof. The detail is as follows.

For (1), we may suppose that O_i and O_j are connected to same X mark point, say X_l . Define a map $H_{X_l} : CFK^-(g) \rightarrow CFK^-(g)$ by

$$H_{X_l}(\mathbf{x}) = \sum_{\mathbf{y} \in \mathcal{S}} \sum_{\{r \in \text{Rect}^\circ(\mathbf{x}, \mathbf{y}) \mid \text{Int}(r) \cap \mathbb{X} = X_l\}} \prod_{t=1}^{2n+k} U_t^{n_{O_t}(r)} \mathbf{y}.$$

Now we want to analyze how $\partial^- \circ H_{X_l} + H_{X_l} \circ \partial^-$ acts on generators. Note that this is a sum of composition of rectangle counting maps so **Remark 3.3** applies. For each pair of $\mathbf{x} \neq \mathbf{z}$ differ by at most four points and each positive domain D connecting them that intersects \mathbb{X} in X_l once, there can only be zero or two ways to decompose D into two rectangles. In case of two, say $D = r_1 * r_2 = r'_1 * r'_2$, then we must have one of r_1, r_2 containing X_l , the other does not, and same hold for r'_1 and r'_2 . Thus, the two decompositions both contribute to $\partial^- \circ H_{X_l} + H_{X_l} \circ \partial^-$ and get canceled mod 2. When $\mathbf{x} = \mathbf{z}$, only two thin annuli through X_l contribute to the map, which gives rise to the term $(U_i - U_j)\mathbf{x}$. Thus

$$\partial^- \circ H_{X_l} + H_{X_l} \circ \partial^- = U_i - U_j,$$

showing the desired homotopy relationship.

For (2), assume we are considering XX_1 . We only need to modify the definition of H into

$$H_{XX_1}(\mathbf{x}) = \sum_{\mathbf{y} \in \mathcal{S}} \sum_{\{r \in \text{Rect}^\circ(\mathbf{x}, \mathbf{y}) \mid \text{Int}(r) \cap \mathbb{X} = XX_1\}} \prod_{t=1}^{2n+k} U_t^{n_{O_t}(r)} \mathbf{y}.$$

Again, all the other terms in $\partial^- \circ H_{XX_1} + H_{XX_1} \circ \partial^-$ cancel in pairs, only the two thin annuli through XX_1 contribute multiplication by $U_i U_j - U_s U_l$. That is

$$\partial^- \circ H_{XX_1} + H_{XX_1} \circ \partial^- = U_i U_j - U_s U_l,$$

showing the desired homotopy relationship. □

Proposition 3.7. *For g as described above, we have an isomorphism of relatively graded vector spaces*

$$\widetilde{HFK}(L) = \widehat{HFK}(L) \otimes W^{\otimes k-m},$$

in which W is a 2-dimensional bigraded vector space spanned by generators in bigrading $(0,0)$ and $(-1,-1)$.

Proof. A basic but important observation is that when multiplication by U_i and U_j are homotopic maps, so when U_i is set to be zero, U_j induces a zero map on homology of the new chain complex.

This observation together with the exact sequence of chain complex (we abbreviate the chain group as C)

$$0 \rightarrow \frac{C}{U_1 = \dots = U_{2n+m} = 0} \xrightarrow{U_{2n+m+1}} \frac{C}{U_1 = \dots = U_{2n+m} = 0} \rightarrow \frac{C}{U_1 = \dots = U_{2n+m+1} = 0} \rightarrow 0$$

leads to a short exact sequence between different homology groups:

$$0 \rightarrow H_*\left(\frac{C}{U_1 = \dots = U_{2n+m} = 0}\right) \rightarrow H_*\left(\frac{C}{U_1 = \dots = U_{2n+m} = U_{2n+m+1} = 0}\right) \rightarrow H_*\left(\frac{C}{U_1 = \dots = U_{2n+m} = 0}\right) \rightarrow 0,$$

in which the second arrow is homogeneous and the third one is of bigrading $(1,1)$.

Then the proof is finished by repeating for each O with subscript greater than $2n+m$. □

3.4. Computing examples. In this subsection, we compute $\widetilde{HFK}(K)$ for some singular knots in $L(2,1)$ and $L(3,1)$.

In **Figure 15**, we show two grid diagrams for a singular knot K_1 with one thick edge in $L(2,1)$ of grid number three and two, respectively. We shall denote the diagrams by g_a and g_b as we labeled in the figure. In g_a , we have forty-eight generators and fifty-six rectangles without any mark points in their interiors. In g_b , we have eight generators and three rectangles without any mark points in their interiors. Using some computer program, we compute that

$$\widetilde{HFK}(g_a) \cong \mathbb{F}^8,$$

with four generators in each $Spin^c$ structure and

$$\widetilde{HFK}(g_b) \cong \mathbb{F}^4,$$

with two generators in each $Spin^c$ structure.

This demonstrate the computable aspect of our theory and also verifies the rank formula in **Proposition 3.7**.

In **Figure 16**, we show a grid diagram g for a singular knot K_2 with one thick edge in $L(3,1)$ of grid number two. In g , we have eighteen generators and ten rectangles without any mark points in their interiors. With the help of some computer program, we compute that

$$\widetilde{HFK}(g) \cong \mathbb{F}^6,$$

with two generators in each $Spin^c$ structure.

We can appeal to **Proposition 3.7** and conclude that

$$\widehat{HFK}(L(2,1), K_1) = \mathbb{F} \oplus \mathbb{F},$$

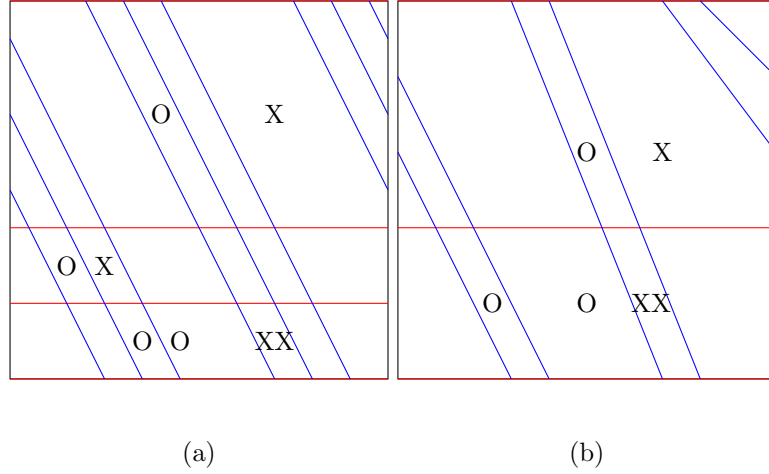


FIGURE 15. Two grid diagrams for a singular knot with one thick edge in $L(2,1)$

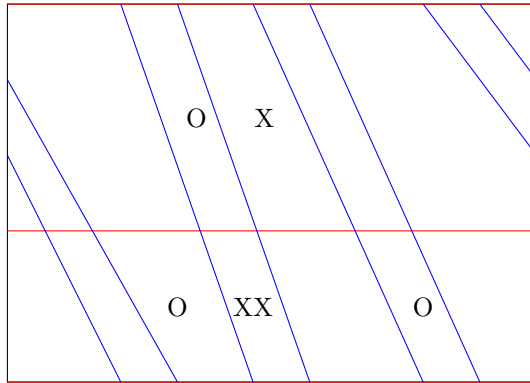


FIGURE 16. A grid diagram for a singular knot with a single thick edge in $L(3,1)$

with one \mathbb{F} from each $Spin^c$ structure and

$$\widehat{HFK}(L(3,1), K_2) = \mathbb{F} \oplus \mathbb{F} \oplus \mathbb{F},$$

with one \mathbb{F} from each $Spin^c$ structure;

3.5. Proof of invariance. Using **Theorem 2.15** in **Subsection 2.4**, we only need to show that if g and g' are two grid diagrams that differ by a commutation or stabilization, then $CFK^\circ(g)$ and $CFK^\circ(g')$ are quasi-isomorphic bigraded chain complexes, for $\circ = \widehat{}$ or $-$. That is

Theorem 3.8. *Fix a singular link L in some lens space $L(p, q)$ as above. If g_1, g_2 are grid diagram for $(L(p, q), L)$, then we have quasi-isomorphisms*

- $CFK^-(g_1) \simeq CFK^-(g_2)$;

- $\widehat{CFK}(g_1) \simeq \widehat{CFK}(g_2)$,

as relatively bigraded chain complexes of modules over $\mathbb{F}[U_1, \dots, U_{2n+m}]$ and over \mathbb{F} respectively. In particular, we have well-defined homology theories for singular links in lens spaces:

- Unblocked grid homology: $HF\widehat{K}^-(L)$ as relatively bigraded modules over $\mathbb{F}[U_1, \dots, U_{2n+m}]$ and
- Simply block grid homology: $\widehat{HF\widehat{K}}(L)$ as relatively bigraded modules over \mathbb{F} .

Since \widehat{CFK} appears as a quotient of $CF\widehat{K}^-$, the proof is easier and similar. We will focus on the second one.

3.5.1. *Commutation invariance.* We will use an important observation in [12]: the existence of line segments LS_1 and LS_2 leads to a well-defined “combined” grid diagram. That is when g and g' differ by a single commutation move, we can combine the information of g and g' into a single diagram. See **Figure 17** for examples, the left two pictures show g and g' , the right pictures show the combined grid diagram and those polygons we shall use later.

Here we illustrate how to modify the proof of [26] into our case for column commutation, the row case is exactly the same. Here we use γ to denote those β -curves after commutation.

Now we introduce the notion of a pentagon on a combined grid diagram. For $\mathbf{x} \in \mathcal{S}(g)$ and $\mathbf{y}' \in \mathcal{S}(g')$ satisfying $|\mathbf{x} \cap \mathbf{y}'| = n + k - 2$, say $x_i = y'_i$ for $i \geq 3$, a pentagon p connecting \mathbf{x} to \mathbf{y}' is one embedded in the combined diagram with

- Four corners of p at $\{x_1, x_2, y'_1, y'_2\}$ respectively;
- Each corner point \mathbf{x} of p is an intersection between two curves from $\{\beta_t, \alpha_t, \gamma_t\}_{t=1}^{n+k}$. A small disk centered at \mathbf{x} is divided into four quadrants by these two curves and p contains exactly one of them.
- $\partial_\alpha p = \partial p \cap \alpha = \mathbf{y}' - \mathbf{x}$.

$Pent(\mathbf{x}, \mathbf{y}')$ will denote the set of pentagons from \mathbf{x} to \mathbf{y}' . A pentagon p is empty if $int(p) \cap \mathbf{x} = \emptyset$. The set of empty pentagons from \mathbf{x} to \mathbf{y}' will be denoted by $Pent^\circ(\mathbf{x}, \mathbf{y}')$. Set $Pent(\mathbf{x}, \mathbf{y}') = \emptyset$, if $|\mathbf{x} \cap \mathbf{y}'| \neq n + k - 2$. Similarly, we can define a pentagon from \mathbf{y}' to \mathbf{x} . One can see directly from the definition that in the first case, p must have a corner point at \mathbf{a} , while in the second case p must have a corner point at \mathbf{b} . See **Figure 17** (c) for examples.

In [12], they used the condition “having all corners less than 90° ” to characterize the convexity of a pentagon. This is equivalent to the second condition in our definition.

Define a $\mathbb{F}[U_1, \dots, U_{2n+k}]$ module map $P : CF\widehat{K}^-(g) \rightarrow CF\widehat{K}^-(g')$ by

$$P(\mathbf{x}) = \sum_{\mathbf{y}' \in \mathcal{S}(g')} \sum_{\{p \in Pent^\circ(\mathbf{x}, \mathbf{y}') \mid p \cap \mathbb{X} = \emptyset\}} \prod_{i=1}^{2n+k} U_i^{n_{o_i}(p)} \mathbf{y}'.$$

Similarly, one defines $P' : CF\widehat{K}^-(g') \rightarrow CF\widehat{K}^-(g)$.

To show that $CF\widehat{K}^-(g)$ and $CF\widehat{K}^-(g')$ are quasi-isomorphic, we check that P is a chain homotopy equivalence with P' as its homotopy inverse. The routine check of P and P' being chain maps has been done in [26] when the background manifold is S^3 and in [12] when the link is regular in lens spaces, we fit their proof into our setup. For any pair of generators $\mathbf{x} \in \mathcal{S}(g)$ and $\mathbf{z}' \in \mathcal{S}(g')$, we consider for each domain D that intersect \mathbb{X} emptily from \mathbf{x} to \mathbf{z}' , how many ways it can be decomposed into an empty rectangle union an empty pentagon. That is, we need to consider $N'(D)$

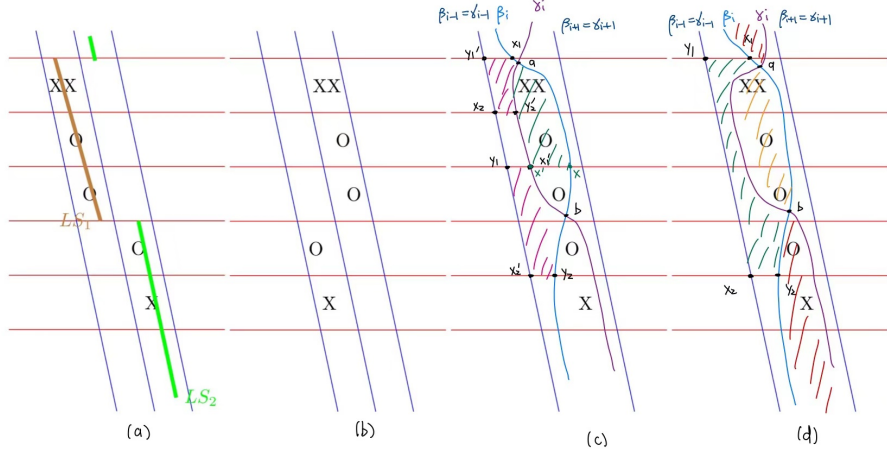


FIGURE 17. **Commutation move and combined grid diagram.** In all pictures here, α -curves are in red and β curves are in blue. In the combined diagrams, we use γ to denote the β curves after commutation. We have $\gamma_j = \beta_j$ for $j \neq i$, and γ_i is drawn in purple which intersect β transversely in two points a and b. In (a) and (b), we draw g and g' , respectively. The brown and green segments in (a) are LS_1 and LS_2 , respectively, showing the commutation is available between these two columns. (c) and (d) are two copies of combined grid diagram for this commutation. In (c), we mark two pentagons in pink: the upper one with a corner at a contributes to P , the lower one with a corner at b contributes to P' . Also in (c), we show a small triangle from \mathbf{x} to the nearest \mathbf{x}' in green. In (d), we show a hexagon in green that contributes to the map H and also two bigons with corners a,b in orange and red.

in

$$\partial^- \circ P(\mathbf{x}) + P \circ \partial^-(\mathbf{x}) = \sum_{\mathbf{z}' \in S(g')} \sum_{D \in \pi(\mathbf{x}, \mathbf{z}')} N'(D) \prod_{i=1}^{2n+k} U^{O_i(r)} \mathbf{z}'.$$

Now $M = |\mathbf{x} - \mathbf{x} \cap \mathbf{z}'|$ may be 1, 2, 3 or 4. The case $M=1$ is ruled out since in this case only thin annulus with a small triangle removed contribute, which always contains a forbidden X ro XX. The case $M=3$ or 4 can be analyzed as in Lemma 5.1.4 of [26]. The case $M=2$ is special for lens spaces. It follows from the proof of $\partial^2 = 0$ in [6] and the observation that by adding a canonical triangle $t_{\mathbf{x}}$ to the pentagon we can reduce the problem to decomposing a domain into juxtaposition of two rectangles. So $N'(D)$ will always be even, thus $\partial^- \circ P + P \circ \partial^- = 0$. The proof for P' is the same. See Section 5.1 of [26] for diagrams illustrating this fact.

We also introduce a hexagon-counting map H as follows: For $\mathbf{x}, \mathbf{y} \in S(g)$, an embedded disk h in the torus with boundary on $\{\beta_t, \alpha_t, \gamma_t\}_{t=1}^{n+k}$ is called a hexagon from \mathbf{x} to \mathbf{y} if

- Four corners of h are in $\mathbf{x} \cup \mathbf{y}$, two other corners are at a, b respectively;

- Each corner point \mathbf{x} of h is an intersection between two curves from $\{\beta_t, \alpha_t, \gamma_t\}_{t=1}^{n+k}$. A small disk centered at \mathbf{x} is divided into four quadrants by these two curves, h contains exactly one of them.
- $\partial_\alpha h = \partial h \cap \alpha = \mathbf{y} - \mathbf{x}$.

As for pentagons, we introduce $Hex(\mathbf{x}, \mathbf{y})$ and $Hex^\circ(\mathbf{x}, \mathbf{y})$ to denote the set of hexagons and empty hexagons from \mathbf{x} to \mathbf{y} . We define $H : CFK^-(g) \rightarrow CFK^-(g)$ by

$$H(\mathbf{x}) = \sum_{\mathbf{y} \in \mathcal{S}(g)} \sum_{\{h \in Hex^\circ(\mathbf{x}, \mathbf{y}) \mid h \cap \mathbb{X} = \emptyset\}} \prod_{i=1}^{2n+k} U_i^{n_{o_i}(h)} \mathbf{y}.$$

This appears naturally as a chain homotopy equivalence between $P' \circ P$ and $id_{CFK^-(g)}$, that is

$$\partial^- \circ H + H \circ \partial^- = P' \circ P - id_{CFK^-(g)}.$$

This identity is shown by considering decomposition of domains into a rectangle union a hexagon or two pentagons. For any $\mathbf{x} \in \mathcal{S}(g)$, we have

$$\partial^- \circ H(\mathbf{x}) + H \circ \partial^-(\mathbf{x}) - P' \circ P(\mathbf{x}) = \sum_{\mathbf{z} \in \mathcal{S}(g)} \sum_{\pi(\mathbf{x}, \mathbf{z})} N''(D) \prod_{i=1}^{2n+k} U_i^{n_{o_i}(D)} \mathbf{z},$$

where $N''(D)$ is number of decomposition of D into the form $r * h$, $p' * p$ or $h * r'$. As the proof of P being a chain map, the case $M = |\mathbf{x} - \mathbf{x} \cap \mathbf{z}'|$ is 0, 3 or 4 has been considered in [26], while the case $M=2$ can be reduced to the rectangle case by adding or deleting suitable bigon from D . In conclusion, $N''(D)$ is even whenever $\mathbf{z} \neq \mathbf{x}$ and $N''(D) = 1$ when D is a thin annulus from \mathbf{x} to \mathbf{x} without any mark point in it. (See Figure 5.9 in [26].) Each \mathbf{x} admits a unique annulus as such. So we can conclude that

$$\partial^- \circ H + H \circ \partial^- = P' \circ P - id_{CFK^-(g)}.$$

It remains to see the relative bigradings are also link invariants, that is P , P' and H are bigraded and of certain bi-grading, respectively. This is not immediate from the existing argument since our grading convention is a little bit complicated. We remedy this by lifting to the universal cover and then applying the existing result. This idea comes from the identification between combinatorially defined Maslov grading and original Maslov grading in [2].

It is well-known that S^3 is the universal cover of $L(p, q)$ with $\mathbb{Z}/p\mathbb{Z}$ as deck transformation group. Denote the covering map by π . L can be lifted to $\tilde{L} = \pi^{-1}(L)$, which is a singular link in S^3 , with possibly more components than L . Note that our function \tilde{W} takes the grid diagram g of L to a grid diagram \tilde{g} of \tilde{L} . Figure 8 of [2] gives a good illustration of this fact.

For any $\mathbf{x} \in \mathcal{S}(g)$, it has a well-defined lift $\tilde{\mathbf{x}} \in \mathcal{S}(\tilde{g})$. By definition of \tilde{W} , we have

$$M(\tilde{\mathbf{x}}) - M(\tilde{\mathbf{y}}) = p(M(\mathbf{x}) - M(\mathbf{y})),$$

whenever \mathbf{x} and \mathbf{y} belong to same $Spin^c$ structure.

For $\mathbf{x} \in \mathcal{S}(g)$, there is a unique $\mathbf{x}' \in \mathcal{S}(g')$ sharing $n+k-1$ points with \mathbf{x} . There is a small triangle $t_{\mathbf{x}}$ connecting them on the combined Heegaard diagram. See **Figure 17**. Consider any $\mathbf{y}' \in \mathcal{S}(g')$ and $p \in Pent^\circ(\mathbf{x}, \mathbf{y}')$ which intersects \mathbb{X} in an empty set. Lifting all these to $\tilde{g}(g')$, the argument of Lemma 5.1.3 in [26] shows that

$$(11) \quad M(\tilde{\mathbf{x}}) - M(\tilde{\mathbf{x}}') = -p + 2|\tilde{t}_{\mathbf{x}} \cap \tilde{\mathbb{O}}| - 2|\tilde{t}_{\mathbf{x}} \cap \tilde{\mathbb{X}\mathbb{X}}|,$$

$$(12) \quad M(\tilde{\mathbf{x}}') - M(\tilde{\mathbf{y}}') = p - 2|\tilde{p} * \tilde{t}_{\mathbf{x}} \cap \tilde{\mathbb{O}}| + 2|\tilde{p} * \tilde{t}_{\mathbf{x}} \cap \tilde{\mathbb{X}\mathbb{X}}|$$

Here we add $\tilde{}$ to each set of points to denote its lift to S^3 .

More precisely, p and $t_{\mathbf{x}}$ each lifts to a disjoint union of p identical copies of pentagons/ triangles in the lift of the combined diagram to S^3 . We can compute directly that

$$\mathcal{J}(\tilde{\mathbf{x}}, \tilde{\mathbf{x}}) - \mathcal{J}(\tilde{\mathbf{x}'}, \tilde{\mathbf{x}'}) = 0$$

$$\mathcal{J}(\tilde{\mathbb{O}} - \tilde{\mathbb{X}\mathbb{X}}, \tilde{\mathbb{O}} - \tilde{\mathbb{X}\mathbb{X}}) - \mathcal{J}(\tilde{\mathbb{O}}' - \tilde{\mathbb{X}\mathbb{X}'}, \tilde{\mathbb{O}}' - \tilde{\mathbb{X}\mathbb{X}'}) = -p,$$

while

$$\mathcal{J}(\tilde{\mathbb{O}} - \tilde{\mathbb{X}\mathbb{X}}, \tilde{\mathbf{x}}) - \mathcal{J}(\tilde{\mathbb{O}}' - \tilde{\mathbb{X}\mathbb{X}'}, \tilde{\mathbf{x}'}) = 0 \text{ or } -p,$$

the value in the last equation changes accordingly with $|t_{\mathbf{x}} \cap (\mathbb{O} \cup -\mathbb{X}\mathbb{X})|$. From this, **Equation 11** follows.

Next, observe that $p * t_{\mathbf{x}}$ is a rectangle from \mathbf{x}' to \mathbf{y}' , which lifts to a union of p rectangles connecting $\tilde{\mathbf{x}'}$ to $\tilde{\mathbf{y}'}$, then **Equation 12** follows from the definition of M .

Now one sees

$$M(\tilde{\mathbf{x}}) - M(\tilde{\mathbf{y}'}) = -2|\tilde{p} \cap \tilde{\mathbb{O}}|,$$

since $p \cap \mathbb{X}\mathbb{X} = \tilde{p} \cap \tilde{\mathbb{X}\mathbb{X}} = \emptyset$.

This together with the covering formula of M show that P preserves M . A similar argument using $M_{\mathbb{X}}$ in place of $M_{\mathbb{O}}$ shows that P preserves $M_{\mathbb{X}}$ also, thus it preserves A . Now we can conclude P is bigraded. Exchange the roles of g and g' , the argument above shows also P' is bigraded.

Using the same idea, we can argue that H is homogeneous of degree $(1,0)$. Again, we illustrate the idea using Maslov grading. If h is a hexagon in $Hex^{\circ}(\mathbf{x}, \mathbf{y})$, then $h * B$ is a rectangle from \mathbf{x} to \mathbf{y} in which B is one of the bigons with corners at a, b (See **Figure 17** (d)). This rectangle lifts to disjoint union of rectangles in \tilde{g} while the bigon B contains a pair of \mathbb{O}, \mathbb{X} or a triple $\{\mathbb{O}, \mathbb{O}, \mathbb{X}\mathbb{X}\}$. Thus

$$M(\tilde{\mathbf{x}}) - M(\tilde{\mathbf{y}}) = -p - 2|(\tilde{h} * \tilde{B} \cap (\tilde{\mathbb{O}} - \tilde{\mathbb{X}\mathbb{X}}))| = p(-1 - 2|h * B \cap (\mathbb{O} - \mathbb{X}\mathbb{X})|),$$

showing that H increases M by 1.

Now we have verified the grading problem, so we can conclude that when g and g' are grid diagrams differ by a commutation, $CFK^{-}(g) \simeq CFK^{-}(g')$ are quasi-isomorphic relatively bigraded chain complexes while $HFK^{-}(g) \cong HFK^{-}(g')$ are isomorphic relatively bigraded modules over $\mathbb{F}[U_1, \dots, U_{2n+m}]$. Thus, we can conclude commutation invariance of our homology theories.

In fact, our proof of grading shift property can be used to show the following lemma.

Lemma 3.9. (Proposition 2.11 of [6], see also Proposition 4.4 of [30]) *If $\mathbf{x}, \mathbf{y} \in \mathcal{S}$ can be connected by $r \in Rect^{\circ}(\mathbf{x}, \mathbf{y})$, then we have*

$$M(\mathbf{x}, \mathbf{y}) = 1 + 2\sum_{i=1}^n n_{\mathbb{X}\mathbb{X}_i}(r) - 2\sum_{i=1}^{2n+k} n_{\mathbb{O}_i}(r),$$

$$A(\mathbf{x}, \mathbf{y}) = 2\sum_{i=1}^n n_{\mathbb{X}\mathbb{X}_i}(r) + \sum_{i=1}^k n_{\mathbb{X}_i}(r) - \sum_{i=1}^{2n+k} n_{\mathbb{O}_i}(r).$$

With the help of this, we can avoid detailed computation as above in the following sections.

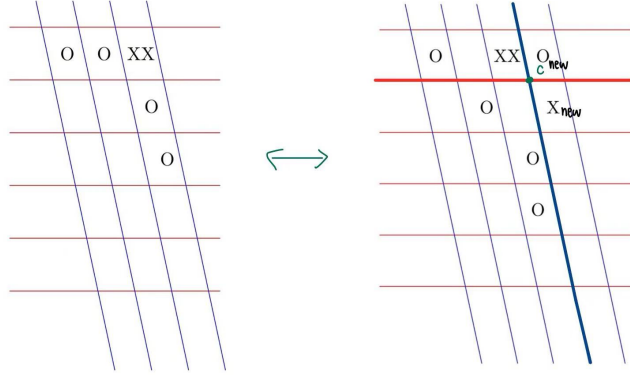


FIGURE 18. **Stabilization.** On the left, we show part of a grid diagram; on the right we show the result after a $XX : SW$ stabilization. The newly introduced curves are bolder than the old ones and the special intersection point c is marked in green.

3.5.2. *Stabilization invariance.* Corollary 3.2.3 in [26] can be reinterpreted in our terminology as follows:

Lemma 3.10. *Any stabilization can be realized as a composition of a stabilization of type $XX : SW$ or $X : SW$ with a sequence of commutations.*

With the help of this lemma, it suffices for us to show that when diagrams g and g' can be related by one such stabilization, $CFK^-(g)$ and $CFK^-(g')$ are quasi-isomorphic as chain complexes of $\mathbb{F}[U_1, \dots, U_{m+2n}]$ modules.

In **Figure 18**, we show a pair of grid diagrams g and g' which differ by a stabilization of type $XX : SW$. For further reference, we call the newly introduced mark points O_{new} and X_{new} . When we do $X : SW$ stabilization, we can not tell which X near O_{new} is the new one, we choose the one sharing same column with O_{new} to be X_{new} . We will need some algebraic terminology in our argument, for detail of this, one can refer to section 5.2.2 of [26].

The intersection point c of newly introduced β and α curve as shown in **Figure 18** will lie in the heart of our argument. Among p intersection points, we specify c to be the corner shared by the new X mark and the XX (or X) at which we do stabilization at.

To achieve our goal, we first deal with the base ring change, as there is a new variable U_{new} in the base ring of $CFK^-(g')$ accounting for O_{new} .

Proposition 3.11. *Suppose that g and g' are given as above, of size $n+k$ and $n+k+1$ respectively. Take U_j to be the variable corresponding to any O_j originally in g and lying in the same thin edge or S^1 component as O_{new} . Then there is a quasi-isomorphism of bigraded chain complexes over $\mathbb{F}[U_{new}, U_1, \dots, U_{2n+k}]$ from $CFK^-(g')$ to $Cone(U_{new} - U_j)$, where $Cone(U_{new} - U_j)$ is the mapping cone of multiplication by $U_{new} - U_j$ on $CFK^-(g)[U_{new}]$.*

This proposition together with an algebraic lemma will complete our proof.

Lemma 3.12. *Let C be a bigraded chain complex over $\mathbb{F}[U_1, \dots, U_{2n+k}]$. Then there is an isomorphism of bigraded $\mathbb{F}[U_1, \dots, U_{2n+k}]$ -modules*

$$H(\text{Cone}(U_{new} - U_j : C[U_{new}] \rightarrow C[U_{new}])) \cong H(C).$$

Here U_j is chosen as in **Proposition 3.11**. This lemma follows from Lemma 5.2.16 of [26] with only some notation changes.

It follows from **Proposition 3.6** that the choice of U_j here is irrelevant to the quasi-isomorphism result.

Using the special intersection point c , we split $\mathcal{S}(g')$ into $\mathbf{I} \cup \mathbf{N}$, where \mathbf{I} is the set of generators containing c and \mathbf{N} is its complement. Let \mathbf{I}^- and \mathbf{N}^- denote the submodule of $CFK^-(g')$ generated by \mathbf{I} and \mathbf{N} , respectively. Since we block all X-marks in our theory, \mathbf{N}^- is actually a subcomplex. Now the differential on $CFK^-(g')$ can be written in matrix form

$$\partial^- = \begin{pmatrix} \partial_{\mathbf{I}}^{\mathbf{I}} & 0 \\ \partial_{\mathbf{I}}^{\mathbf{N}} & \partial_{\mathbf{N}}^{\mathbf{N}} \end{pmatrix},$$

so $CFK^-(g')$ is the mapping cone of $\partial_{\mathbf{I}}^{\mathbf{N}} : (\mathbf{I}^-, \partial_{\mathbf{I}}^{\mathbf{I}}) \rightarrow (\mathbf{N}^-, \partial_{\mathbf{N}}^{\mathbf{N}})$.

Note that one has a natural bijection $c : \mathcal{S}(g) \rightarrow \mathbf{I}$, $\mathbf{x} \mapsto \mathbf{x}' = \mathbf{x} \cup \{c\}$. This c leads to an isomorphism of chain complexes $e : (\mathbf{I}^-, \partial_{\mathbf{I}}^{\mathbf{I}}) \rightarrow CFK^-(g)[U_{new}][1, 1]$. Here and below, we use $C[l, k]$ to denote the complex C with bigrading (M, A) shifted up by (l, k) . The proof of this fact follows immediately from the natural bijection on the sets of generators and rectangles.

Again, we need to deal with the grading problem. On one hand, we can lift the singular link L as well as diagrams g and g' via π to \tilde{L} , \tilde{g} and \tilde{g}' . Using the fixed absolute lift, one can compute directly $M(\tilde{\mathbf{x}}') - M(\tilde{\mathbf{x}}) = -p$, $A(\tilde{\mathbf{x}}') - A(\tilde{\mathbf{x}}) = -p$ using the combinatorial formula, which is straight forward in S^3 case. On the other hand, we can appeal to **Lemma 3.9** and see the grading shift in a direct way.

Now we introduce rectangle-counting maps to relate $(\mathbf{I}^-, \partial_{\mathbf{I}}^{\mathbf{I}})$ and $(\mathbf{N}^-, \partial_{\mathbf{N}}^{\mathbf{N}})$. Define

- $H_{X_{new}} : \mathbf{N}^- \rightarrow \mathbf{I}^-$ by

$$H_{X_{new}}(\mathbf{x}) = \sum_{\mathbf{y} \in \mathbf{I}} \sum_{\{r \in \text{Rect}^\circ(\mathbf{x}, \mathbf{y}) \mid \text{int}(r) \cap \mathbb{X} = X_{new}\}} \prod_{i=1}^{2n+k} U_i^{n_{O_i}(r)} \cdot U_{new}^{n_{O_{new}}(r)} \mathbf{y}.$$

- $H_{O_{new}} : \mathbf{I}^- \rightarrow \mathbf{N}^-$ by

$$H_{O_{new}}(\mathbf{x}) = \sum_{\mathbf{y} \in \mathbf{N}} \sum_{\{r \in \text{Rect}^\circ(\mathbf{x}, \mathbf{y}) \mid \text{int}(r) \cap \mathbb{X} = \emptyset, O_{new} \in \text{int}(r)\}} \prod_{i=1}^{2n+k} U_i^{n_{O_i}(r)} \mathbf{y}.$$

- $H_{X_{new}, O_{new}} : \mathbf{N}^- \rightarrow \mathbf{N}^-$ by

$$H_{X_{new}, O_{new}}(\mathbf{x}) = \sum_{\mathbf{y} \in \mathbf{N}} \sum_{\{r \in \text{Rect}^\circ(\mathbf{x}, \mathbf{y}) \mid \text{int}(r) \cap \mathbb{X} = X_{new}, O_{new} \in \text{int}(r)\}} \prod_{i=1}^{2n+k} U_i^{n_{O_i}(r)} \mathbf{y}.$$

Since all three maps concern generators in the grid diagram g' , we can verify directly using the lifted diagram \tilde{g}' that $H_{X_{new}}$, $H_{O_{new}}$ and $H_{X_{new}, O_{new}}$ are of bi-grading $(-1, -1)$, $(1, 1)$ and $(1, 0)$ respectively. We can also appeal to **Lemma 3.9** and prove the grading shift formula by counting mark points in rectangles that are taken into account in each map.

It can be shown as in [30] that

Lemma 3.13. $H_{X_{new}}, H_{O_{new}}$ are chain maps:

$$\partial_{\mathbf{I}}^{\mathbf{I}} \circ H_{X_{new}} = H_{X_{new}} \circ \partial_{\mathbf{N}}^{\mathbf{N}},$$

$$\partial_{\mathbf{N}}^{\mathbf{N}} \circ H_{O_{new}} = H_{O_{new}} \circ \partial_{\mathbf{I}}^{\mathbf{I}}.$$

As we have discussed during the proof of $\partial^2 = 0$, we consider for each pair of generators (\mathbf{x}, \mathbf{z}) in \mathbf{N} or \mathbf{I} and each domain D from \mathbf{x} to \mathbf{z} how many times it contributes to $H_{X_{new}} \circ H_{O_{new}}$ and $H_{O_{new}} \circ H_{X_{new}} + \partial_{\mathbf{N}}^{\mathbf{N}} \circ H_{X_{new}, O_{new}} + H_{X_{new}, O_{new}} \circ \partial_{\mathbf{N}}^{\mathbf{N}}$. For $H_{X_{new}} \circ H_{O_{new}}$, our life is easy since only thin annuli involve, contribute $\mathbf{x} \mapsto \mathbf{x}$ for each $\mathbf{x} \in \mathbf{I}$. In case of \mathbf{N} , note that all maps in these terms are rectangle counting maps, so **Remark 3.3** applies. In each decomposition $D = r_1 * r_2$, it contributes to one of the four terms depending on how O_{new} and X_{new} distribute in the two rectangles. So $N(D) = 2$ except the case that D is the thin annulus through X_{new} and O_{new} . Such an annulus contributes $\mathbf{x} \mapsto \mathbf{x}$ for every $\mathbf{x} \in \mathbf{N}$. These together show identities:

$$\begin{aligned} H_{X_{new}} \circ H_{O_{new}} &= Id_{\mathbf{I}^-}; \\ H_{O_{new}} \circ H_{X_{new}} + \partial_{\mathbf{N}}^{\mathbf{N}} \circ H_{X_{new}, O_{new}} + H_{X_{new}, O_{new}} \circ \partial_{\mathbf{N}}^{\mathbf{N}} &= Id_{\mathbf{N}^-}. \end{aligned}$$

Combining computations above, we have a commutative square

$$\begin{array}{ccc} (\mathbf{I}^-, \partial_{\mathbf{I}}^{\mathbf{I}}) & \xrightarrow{\partial_{\mathbf{I}}^{\mathbf{N}}} & (\mathbf{N}^-, \partial_{\mathbf{N}}^{\mathbf{N}}) \\ \downarrow e & & \downarrow e \circ H_{X_{new}} \\ (CFK^-(g)[U_{new}][1, 1], \partial_g^-) & \xrightarrow{U_{new} - U_j} & (CFK^-(g)[U_{new}][1, 1], \partial_g^-) \end{array} .$$

This together with Lemma 5.2.12 in [26] (property of mapping cone) lead to **Proposition 3.11**.

Thus, we can conclude that when g and g' are grid diagrams that differ by a single stabilization we have q quasi-isomorphism of relatively bigraded chain complexes $CFK^-(g) \simeq CFK^-(g')$ and an isomorphism of relatively bigraded $\mathbb{F}[U_1, \dots, U_{2n+m}]$ -modules $HFK^-(g) \cong HFK^-(g')$.

In summary, for a singular link L embedded in $L(p, q)$ and any grid diagram g representing it, $HFK^-(L) =: HFK^-(g)$ and $\widehat{HFK}(L) =: \widehat{HFK}(g)$ are well-defined invariants for the isotopy class of L .

Remark 3.14. *In Section 5 of [30], they showed invariance of grid homology for regular lens space links in great detail. Although we did not provide a detailed analysis on decompositions of domains, Remark 3.3 together with their investigation on higher polygons form a complete proof.*

4. RESOLUTION CUBE

Having defined grid homology for singular links in lens spaces, we now try to relate grid homology of links that differ by a local change and provide a way to do computation through grid homology of those links that admit a torus diagram without any crossing (defined as ‘‘totally singular’’ in [25]). More concretely, our main tasks in this section are

- (1) Proving a skein exact sequence, which acts as the foundation of a resolution cube;
- (2) Constructing a spectral sequence starting from the resolution cube and converging to the grid homology of links in lens spaces.

For grid homology of regular links in lens spaces, one can regard regular knots and links as singular ones without vertices or one can refer to [2]. In [2], they also identified the grid homology for regular lens space links with HFL° defined in [24]. So we are actually proving a resolution cube

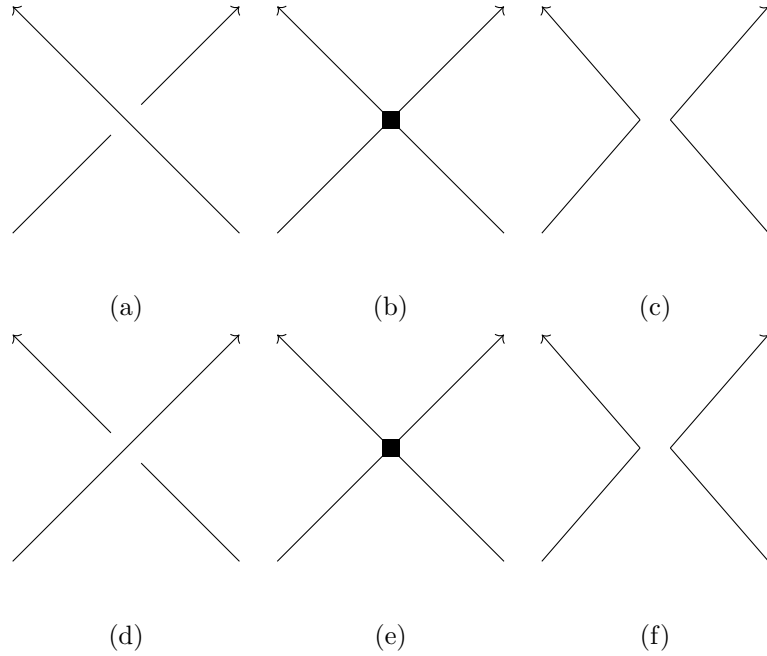


FIGURE 19. **Resolution of crossings.** In (a), we show a negative crossing. In (b), (c) we show its corresponding singularization and smoothing. Similarly, in the second row, we show a positive crossing together with its singularization and smoothing in (d), (e) and (f), respectively.

of HFL° specialized to grid diagrams. The construction in this section mostly follows Section 4 and 6 of [25]. Although all the existing resolution cubes used braid diagrams of knots and links, as remarked in Section 4 of [25], this construction has no dependence on the property of braids.

4.1. Resolution of crossings. For knots in S^3 , it is natural to consider resolution on a planar diagram. In our case, resolving crossings on a torus projection appears as a natural choice. Our singular links appear with orientation, so we can assign a sign to each crossing, see **Figure 19**. For a diagram with oriented crossings, an usual way to form a resolution cube is to consider oriented resolution and disoriented resolution at each crossing. This was used to construct Khovanov homology. However, we will use singularization in place of disoriented resolution and that's where singular links appear.

Definition 4.1. *At each crossing in a torus diagram for a possibly singular link in lens space $L(p, q)$, we define its smoothing and singularization as shown in **Figure 19**. For a positive crossing, we call its smoothing the 1-resolution and its singularization the 0-resolution. For a negative crossing, the notions of 0 and 1 exchange.*

Note that for each pair of X, O marks sharing a row or a column, there are two ways to connect them in the complement of α or β curves. Recall that we cut Σ open along a pair of generic

representatives for a symplectic basis of $H_1(\Sigma; \mathbb{Z})$ to obtain a planar diagram. We fix the convention that on this diagram, those vertical segments emanating from X always go upward diagrammatically. From now on, we mean by g a grid diagram together with a fixed way of connecting base points to obtain the link projection subjected to the above convention. Thus, each positive or negative crossing locally looks like in **Figure 20** (d) or (a). There are certain cells containing crossings in the grid diagram, which will be called crossing squares. To make resolving a crossing available on a grid diagram, we need the assumption of special on diagram in the following sense:

Definition 4.2. (*Definition 6.1 in [25]*) *A grid diagram is called special if*

- (1) *each vertical arc crosses at most one horizontal arc, each horizontal arc goes under at most one vertical arc, i.e each column or row has at most one crossing square;*
- (2) *no two crossing squares share a corner;*
- (3) *each crossing square shares two sides with squares marked by X , the corner shared by the two X -labeled cells will be called the two X s crossing corner;*
- (4) *when a rectangle has two of its corners being crossing corners, it contains an X in the interior.*

Using grid moves, every link in a lens space possesses a special diagram. Indeed, the first two requirements can be achieved by sufficiently many stabilization moves. The third one can be achieved by stabilization and commutations. In **Figure 20**, we define the standard picture at crossings that meets the need of (3) and show how to achieve it for each positive or negative crossing. Our resolution cube will be constructed based on grid diagrams that are special and standard at each crossing. The fourth one is guaranteed once we have (1) and the standard picture of (3) in hand.

Using the standard picture, we can resolve a crossing on a diagram. That is, we can change a diagram locally to get one for the singularized or smoothed link at each crossing. See **Figure 21**.

From now on, we fix a (possibly) singular link L in $L(p, q)$ and choose a grid diagram g_0 of it. We apply the procedure above to get a special grid diagram g . Now, take any of its crossing c . As we did when proving commutation invariance, we can form a combined diagram that contains the information of the original link L and the resolved link L_r . With a little effort, the singularized link L_s can also be reconstructed from this diagram. See **Figure 22**.

For further reference, we fix some notation here: For a grid diagram g , we denote by

- $X(-)$, the set of singular points;
- $C(-)$, the set of crossings.

Note that $X(g)$ depends only on the underlying oriented graph, while $C(g)$ depends on the diagram g itself.

Definition 4.3. *Fix any grid diagram g , a complete resolution is an assignment $I : C(g) \rightarrow \{0, 1\}$, which assigns to each crossing its 0 or 1 resolution. When g is a special grid diagram with the standard local picture as in **Figure 20** at each crossing, we can apply the procedure in **Figure 21** to get a canonical diagram for the resolved link. This will be denoted by g_I for each complete resolution.*

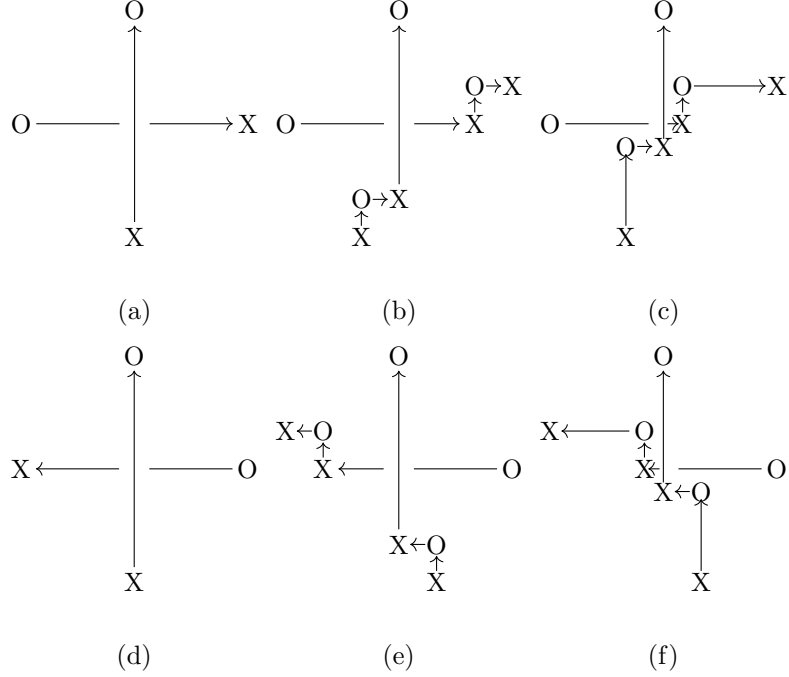


FIGURE 20. **Standard picture at each crossing.** In (a) and (d), we show how a negative and positive crossing will look like after fixing our convention; In (b) and (c), we show how to achieve (3) in the definition of a special grid diagram starting from (a) via a sequence of stabilization and commutation. Similarly, we do for (d) in (e) and (f). The patterns in (c) and (f) are defined to be the standard picture for a negative or positive crossing respectively.

4.2. Skein exact sequence. To form a resolution cube, we first prove the existence of a skein exact sequence.

Theorem 4.4. *Let L , c , g be fixed as above. Denote the resulting grid diagram for smoothing and singularization at c by g_r , g_s and call the corresponding links L_r and L_s , respectively. Let O_a , O_b be marks sharing the same column with the newly formed XX base point, O_c , O_d be marks sharing the same row with the newly formed XX base point. Then we have the following:*

- When c is positive, there is an exact sequence:

$$(13) \quad \dots \longrightarrow \mathrm{HFK}^-(L) \longrightarrow H_*\left(\frac{\mathrm{CFK}^-(L_s)}{U_a + U_b - U_c - U_d}\right) \longrightarrow \mathrm{HFK}^-(L_r) \longrightarrow \mathrm{HFK}^-(L) \longrightarrow \dots$$

- When c is negative, there is an exact sequence:

$$(14) \quad \dots \longrightarrow \mathrm{HFK}^-(L) \longrightarrow \mathrm{HFK}^-(L_r) \longrightarrow H_*\left(\frac{\mathrm{CFK}^-(L_s)}{U_a + U_b - U_c - U_d}\right) \longrightarrow \mathrm{HFK}^-(L) \longrightarrow \dots$$

We will relate the complexes defined by g , g_r and g_s given their close relationship. For further use, we set up more notations:

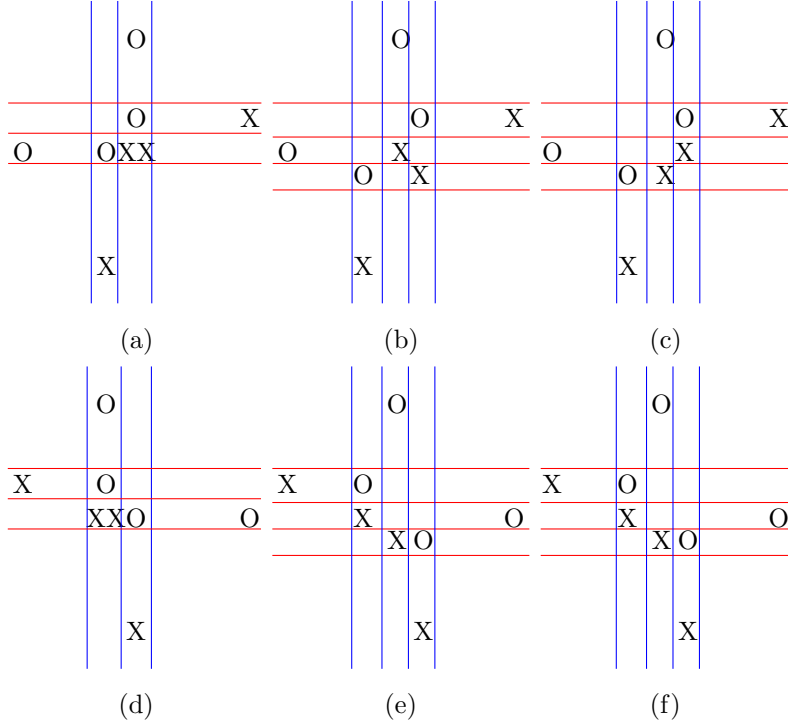


FIGURE 21. **Realizing resolution on grid diagram.** (c) and (f) here are the same as in **Figure 20**. In (b)((e)), we show a grid diagram for the smoothing of the crossing in (c) ((f)). In (a)((d)), we merge the two rows as well as the two columns containing crossing X into one singular row and one singular column. This gives rise to a grid diagram for the singular knot or link after singularizing at this crossing.

- \mathbb{X}_0 will denote the set of all X or XX base points except the two adjacent to the crossing square of c, which is shared by g, g_r and g_s . $\mathbb{X}(-)$ denotes the set of all X and XX base points in a grid diagram.
- \mathbb{O} will denote the set of O base points, shared by g, g_r and g_s .
- \mathbb{B}, \mathbb{A} will denote the set of B, A marks, respectively.

We first assume c is positive. As in the proof of stabilization invariance, the intersection point p at the shared corner of the two X-labeled squares will be of importance. Consider a decomposition $\mathcal{S} = \mathcal{P} \cup \mathcal{C}$, where \mathcal{P} is the set of generators containing p, \mathcal{C} is the complement of \mathcal{P} in \mathcal{S} . Let Z be the submodule of $CFK^-(g_r)$ generated by \mathcal{P} . Z is actually a subcomplex of $CFK^-(g_r)$, since we only allow rectangles without X marks in our differential. Let Y be the quotient complex $CFK^-(g_r)/Z$, then Y has \mathcal{C} as a generating set, and the induced differential on Y counts rectangles without any A, B or X in its interior.

Lemma 4.5. *Z is isomorphic to the chain complex $CFK^-(g_s)$.*

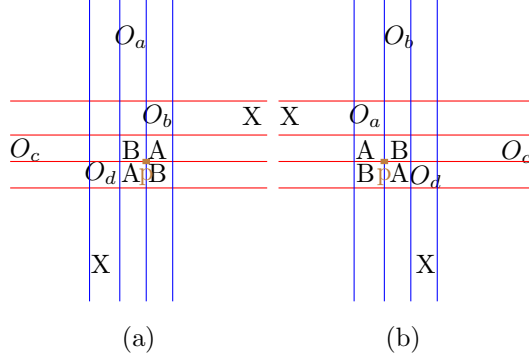


FIGURE 22. **Combined diagram for resolution of crossing.** (a) is a combined diagram for L_r and L when c is a negative crossing. When putting X marks at B 's, we get the grid diagram g_r , while putting X marks at A 's, we get g . By compressing two rows and columns containing A, B into single ones, we get g_s . (b) shows one when c is positive. In both cases, O points are marked as in the description of **Theorem 4.4** and p is the special intersection point we shall use in the proof.

Proof. We shall construct a chain homotopy equivalence $Q : CFK^-(g_s) \rightarrow Z$ as follows. Observe that except the α and β curve meeting at p , and the splitting of a pair of singular column and row into two regular columns and rows g_r is exactly the same as g_s . Thus, we have a bijection $Q : \mathcal{S}(g_s) \rightarrow \mathcal{P}$ given by $\mathbf{x} \mapsto \mathbf{x}' = \mathbf{x} \cup \{p\}$. This leads to a map $Q : CFK^-(g_s) \rightarrow Z$. We claim that it is a chain map. This follows from the observation that we also have a bijection

$$\{\text{rectangles counted by } \partial_{g_s}^-\} \xrightarrow{1:1} \{\text{rectangles counted by } \partial_Z^-\}.$$

Indeed, consider a pair $\mathbf{x}, \mathbf{y} \in \mathcal{S}(g_s)$, for which there is a rectangle r of size $a \times b$ in $Rect^\circ(\mathbf{x}, \mathbf{y})$ that intersects $\mathbb{X}(g_s)$ emptily. Denote the column and row the newly introduced XX belongs to by C_s and R_s . If $\text{int}(r) \cap C_s = \text{int}(r) \cap R_s = \emptyset$, then r has its image r' lives in $Rect^\circ(\mathbf{x}', \mathbf{y}')$ naturally. Note that since $\text{int}(r) \cap \mathbb{X} = \emptyset$, r can not intersect both C_s and R_s . If $\text{int}(r) \cap C_s \neq \emptyset$, then by augmenting the part of size $1 \times b$ in the intersection into a sub-rectangle of size $2 \times b$, we get r' embedding in g_r that belongs to $Rect^\circ(\mathbf{x}', \mathbf{y}')$. Similar operation can be done if $\text{int}(r) \cap R_s \neq \emptyset$. Now we have a well-defined map from the left-hand side to the right-hand side. On the other hand, for any pair $\mathbf{x}', \mathbf{y}' \in \mathcal{P}$ and $r' \in Rect^\circ(\mathbf{x}', \mathbf{y}')$, r' does not have any corner at p and must intersect the four squares with p as a corner emptily. Thus, any such r' gives rise to a unique r in $Rect^\circ(\mathbf{x}, \mathbf{y})$ during the merge of rows and columns. One can see directly this procedure is inverse to the one described above. This shows that $\partial_Z^- \circ Q = Q \circ \partial_{g_s}^-$, i.e. Q is a chain map.

In summary, for Z and $CFK^-(g_s)$, we have a chain map Q induced by one to one correspondence on generators. Thus, they are isomorphic chain complexes. \square

On the other hand, Y appears naturally as a subcomplex of $CFK^-(g)$ with quotient complex $CFK^-(g)/Y$ isomorphic to Z . Define maps $\Phi_A : Y \rightarrow Z$

$$\Phi_A(\mathbf{x}) = \sum_{\mathbf{y} \in \mathcal{P}} \sum_{\{r \in \text{Rect}^\circ(\mathbf{x}, \mathbf{y}) \mid n_{\mathbb{X}_0}(r)=0, n_{\mathbb{A}}(r)=1\}} \prod_{O_i \in \mathbb{O}} U_i^{n_{O_i}(r)} \mathbf{y};$$

and $\Phi_B : Z \rightarrow Y$,

$$\Phi_B(\mathbf{x}) = \sum_{\mathbf{y} \in \mathcal{C}} \sum_{\{r \in \text{Rect}^\circ(\mathbf{x}, \mathbf{y}) \mid n_{\mathbb{X}_0}(r)=0, n_{\mathbb{B}}(r)=1\}} \prod_{O_i \in \mathbb{O}} U_i^{n_{O_i}(r)} \mathbf{y}.$$

These are chain maps again follows from **Remark 3.3**, since Φ_A , Φ_B and ∂_Y^- , ∂_Z^- are all rectangle counting maps.

One can see directly that $CFK^-(g_r)$ appears as the mapping cone of Φ_A , while $CFK^-(g)$ appears as the mapping cone of Φ_B .

Lemma 4.6. *The compositions $\Phi_A \circ \Phi_B$ and $\Phi_B \circ \Phi_A$ are both equal to multiplication by $U_c + U_d - U_a - U_b$.*

Proof. This proof is similar to the one we used in the proof of stabilization invariance but actually easier. For both $\Phi_A \circ \Phi_B$ and $\Phi_B \circ \Phi_A$, the proof is direct. Note that they are both compositions of rectangle counting maps, so **Remark 3.3** applies. So after mod 2 only thin annuli through rows or columns containing a pair of A, B contribute to these compositions. Two horizontal annuli give rise to multiplication by U_c and U_d while two vertical annuli give rise to multiplication by U_a and U_b . Since we are working mod 2, the conclusion follows. \square

When c is a negative crossing, we still have a special point p in our combined diagram. But now Z is a subcomplex of $CFK^-(g)$ with quotient complex Y , while Y is a subcomplex of $CFK^-(g_r)$ with quotient complex Z . For $\Phi_A : Z \rightarrow Y$ and $\Phi_B : Y \rightarrow Z$ defined using similar expressions (except the direction of arrows change), we have $CFK^-(g)$ being the mapping cone of Φ_B , $CFK^-(g_r)$ being the mapping cone of Φ_A . **Lemma 4.5**, **4.6** and their proof work without change.

We now have commutative squares for c , a positive or a negative crossing, respectively:

$$(15) \quad \begin{array}{ccc} Z & \xrightarrow{\Phi_B} & Y \\ \downarrow U_c+U_d-U_a-U_b & & \downarrow \Phi_A \\ Z & \xrightarrow{=} & Z \end{array} \quad \begin{array}{ccc} Z & \xrightarrow{=} & Z \\ \downarrow \Phi_A & & \downarrow U_c+U_d-U_a-U_b \\ Y & \xrightarrow{\Phi_B} & Z \end{array}$$

Proof. (of **Theorem 4.4**) When c is a positive crossing, we have the first diagram above in hand, which is quasi-isomorphic to $\text{Cone}(\Phi_B)$ thus $CFK^-(g)$. This can be seen by considering the filtration by the vertical coordinate, where the complex is an extension of a subcomplex with trivial homology by a quotient complex quasi-isomorphic to $\text{Cone}(\Phi_B)$. On the other hand, using the horizontal filtration, we can regard it as an extension of a subcomplex isomorphic to $\text{Cone}(\Phi_A)$ by $\text{Cone}(U_a + U_b - U_c - U_d)$. Recall that **Lemma 4.5** said that Z is isomorphic to the chain complex $CFK^-(g_s)$. Putting things together, we have a long exact sequence :

$$\dots \rightarrow HFK^-(g) \rightarrow H_*\left(\frac{CFK^-(g_s)}{U_a + U_b - U_c - U_d}\right) \rightarrow HFK^-(g_r) \rightarrow HFK^-(g) \rightarrow \dots,$$

when c is positive.

Arguing using the second diagram, we see that

$$\dots \longrightarrow \mathrm{HFK}^-(g) \longrightarrow \mathrm{HFK}^-(g_r) \longrightarrow H_*\left(\frac{\mathrm{CFK}^-(g_s)}{U_a + U_b - U_c - U_d}\right) \longrightarrow \mathrm{HFK}^-(L) \longrightarrow \dots$$

is exact when c is negative.

Since g_r, g, g_s are diagrams for L_r, L, L_s respectively, we have the desired skein exact sequences. \square

Remark 4.7. *Our proof mimics the one in Section 6 of [25], whose argument in turn follows from the proof using planar diagrams given in Section 4 of the same article. However, under the combinatorial setup, things are actually easier since now $\Phi_A \circ \Phi_B = U_c + U_d - U_a - U_b$, that is, there is no need for a chain homotopy to relate them.*

4.3. Remarks on gradings. We want our skein relation to preserve the relative bigrading on homology groups. Since our definition of grading is somehow complicate, we need a generalization of **Lemma 3.9**.

To show that the skein exact sequence we introduced in the previous section is bigrading preserving, we need to find out how gradings change under the four maps we considered above: Q, Φ_A, Φ_B and multiplication by $U_c + U_d - U_a - U_b$. We will fix the convention that when we say a map is of bi-degree (m, a) , then it increases Maslov grading by m and increases Alexander grading by a . The last one is clearly of bi-degree $(-2, -1)$, so it suffices to consider the first three. We assume here that c is positive so that Z is a subcomplex of $\mathrm{CFK}^-(g_r)$, while Y is a subcomplex of $\mathrm{CFK}^-(g)$. Negative case can be treated in exactly the same way. In this case we have

$$\mathrm{CFK}^-(g_r) \cong \mathrm{Cone}(\Phi_A), \quad \mathrm{CFK}^-(g) \cong \mathrm{Cone}(\Phi_B).$$

Recall that in the construction of Q , we have an explicit correspondence between generators and rectangles. The proof of **Lemma 4.5** shows that if \mathbf{x}, \mathbf{y} in $\mathcal{S}(g_s)$ can be connected by a rectangle without the distinguished XX mark point, then \mathbf{x}', \mathbf{y}' in \mathcal{P} can be connected by a rectangle that changes the bigrading in exactly the same way. (This is obvious when the background manifold is S^3 , when it is some $L(p, q)$, the rectangle lifts to p copies on S^3 using the additivity of all terms in the definition of gradings and the covering formula, one sees the result holds in general.) This shows that Q is a bigraded chain map between relatively bigraded groups.

The identification of grid homology with the usual Heegaard Floer homology has been done in [18]. One can also observe that the grid version of singular knot Floer defined in [25] is the same as ours. These together with Lipshitz formula for Maslov index and **Lemma 3.9** show that for $\mathbf{x}, \mathbf{y} \in \mathcal{S}$ and a rectangle r connecting them, we have

$$M(\mathbf{x}, \mathbf{y}) = 1 + 2n_{\mathrm{XX}}(r) - 2n_{\circlearrowleft}(r) + n_{\mathbf{x}}(\mathrm{int}(r)) + n_{\mathbf{y}}(\mathrm{int}(r)),$$

$$A(\mathbf{x}, \mathbf{y}) = 2n_{\mathrm{XX}}(r) + n_{\mathrm{X}_r}(r) - n_{\circlearrowleft}(r).$$

The notation here follows **Subsection 3.2**.

Also note that if g is a grid diagram for a link in $L(p, q)$, let \tilde{g} be its lift to S^3 , then we have a rectangle embedded in g give rises to p copies of rectangles in \tilde{g} each containing same number of each kind of marks. Thus, regarding Z, Y as sub/quotient complexes of $\mathrm{CFK}^-(g_r)$, Φ_A has bi-degree $(-1, 0)$ while Φ_B has bi-degree $(-1, -1)$. While when regarding Z, Y as quotient/sub complexes of

$CFK^-(g)$, Φ_A has bi-degree $(-1,-1)$ while Φ_B has bi-degree $(-1,0)$. The differences come from the position change of X base points.

Now we have shown that all the maps we used in the construction above are of certain bidegree. Assume c is positive, a closer look at the exact sequence shows that in

$$\longrightarrow HFK^-(g) \longrightarrow H_*\left(\frac{CFK^-(g_s)}{U_c + U_d - U_a - U_b}\right) \longrightarrow HFK^-(g_r) \longrightarrow HFK^-(g) \longrightarrow,$$

the second arrow is induced by a quotient of chain complex, and the third arrow is induced by composition of inclusion, so both of them are grading preserving. Moreover, the fourth arrow comes from $\Phi_A : Y \rightarrow Z$ connecting a quotient complex to a subcomplex that is of bidegree $(-1,0)$ as we seen above.

A similar analysis shows that when c is negative the only grading shift $(-1,0)$ happens at the arrow $HFK^-(g) \rightarrow HFK^-(g_r)$.

There is also a more formal way of seeing the change in Maslov grading, using the fact that M acts as the homological grading in our theories. For any pair of graded chain maps $f : A \rightarrow B$, $g : B \rightarrow C$, we have an exact triangle

$$Cone(f) \longrightarrow Cone(g \circ f) \longrightarrow Cone(g).$$

In the induced long exact sequence, grading change happens at the connected morphism $H_*(Cone(g)) \rightarrow H_*(Cone(f))$. Apply to our case, we have $\frac{CFK^-(g_s)}{U_c + U_d - U_a - U_b}$ being the mapping cone of $U_c + U_d - U_a - U_b = \Phi_A \circ \Phi_B : Z \rightarrow Z$, thus we have the degree shifting property as above.

Remark 4.8. *Recall that on a grid diagram, two generators \mathbf{x}, \mathbf{y} belong to same $Spin^c$ class iff they can be connected by a sequence of rectangles in g . Since Q is defined via a direct identification of generators and differential while Φ -maps are defined by counting rectangles, they all preserve $Spin^c$ class of generators. Therefore, our exact sequence actually splits into p distinct exact sequences, one for each $Spin^c$ class. For more details on $Spin^c$ structure one can refer to [23].*

4.4. Resolution cube and spectral sequence. We shall prove an analogue of Theorem 4.4 in [25] or more precisely, Theorem 1.2 in [16], since we will consider an untwisted resolution cube over the usual base ring $\mathbb{F}[U_1, \dots, U_{2n+m}]$. As remarked at the beginning of Section 2 in [16], they used the twisted coefficient originally in [25] to obtain finiteness on induced maps and to deal with extra components appear in the smoothings. In detail,

- (1) we need all the rectangle counting maps occurring in higher differentials to have a finite coefficient for each generator;
- (2) we need to deal with the change of base ring when one component of L split into two during smoothing of a crossing.

For (1), they used admissibility of diagram to solve the problem in [16]. On a grid diagram, there is no non-trivial periodic domain, i.e. any nonempty domain with boundary a sum of α and β curves must contain some O or X(XX) mark point, so admissibility holds naturally.

They solved (2) by an operation called insertion, i.e. introducing a new pair of α and β curves together with a new pair of O, X base points. Using this, they showed how to deal with the base ring change by the lemma below. Its proof turned out to rely on Lemma 6.1 in [24] which does not require the background manifold to be the three-sphere, thus it holds in our case. Note that on a

special grid diagram with the standard picture at each crossing, we already have sufficiently many base points and variables, so no insertion is needed. One can compare our **Figure 20, 21** with Figure 6 in [24].

Lemma 4.9. (lemma 2.2 of [16] adapted into our setup) *Let L be a possibly singular link in lens space $L(p, q)$ with components L_1, \dots, L_l . For each L_i , we have a chain complex $CFK^-(L_i)$ over some polynomial ring R_i . Some suitable choices of a special grid diagram for each of them can be fit into one of L , so we have $CFK^-(L)$ over*

$$R = R_1 \otimes_{\mathbb{F}} \dots \otimes_{\mathbb{F}} R_l.$$

Then we have quasi-isomorphism of R -modules :

$$CFK^-(L) \sim CFK^-(L_1) \otimes_{\mathbb{F}} \dots \otimes_{\mathbb{F}} CFK^-(L_l) \otimes_{\mathbb{F}} H_*(T^{l-1}).$$

With these two problems solved, we can use the idea from [25] to construct an untwisted resolution cube for links in lens spaces.

To make a precise statement, we need some terminology:

- R will denote the ring $\mathbb{F}[U_1, \dots, U_{2n+k}]$, each U_i corresponding to an O mark O_i . (Here n is the number of XX marks, k is the number of X marks, thus g is of size $n+k$.)
- To each crossing $c \in C(g)$, we denoted by $O_a^{(c)}, O_b^{(c)}$ the O marks that two corner X's point to, while denoted by $O_c^{(c)}, O_d^{(c)}$ the two O marks that point to the pair of corner X's. We introduce similar notation for $XX \in X(g)$. See **Figure 22** for an illustration. Further denote by $u^{(c)}$ the term $U_a^{(c)} + U_b^{(c)} - U_c^{(c)} - U_d^{(c)} \in R$.
- For a crossing $c \in C(g)$, let $g_{c,s}, g_{c,r}$ denote the singularized or smoothed diagram at this single crossing c .
- We define

$$\begin{aligned} \mathcal{U}_c &: CFK^-(g_{c,s}) \otimes_R R/(u^{(c)}) \rightarrow CFK^-(g_{c,r}), \\ \mathcal{Z}_c &: CFK^-(g_{c,r}) \rightarrow CFK^-(g_{c,s}) \otimes_R R/(u^{(c)}) \end{aligned}$$

to be the unzip or zip homomorphism induced by the horizontal arrows in left and right diagrams in **Equation 15**.

The resolution cube of g is the union $\bigcup_{I:C(g) \rightarrow \{0,1\}} g_I$. Using this, we form a relatively bi-graded \mathbb{R} module $V(g) = \bigoplus_I V(g_I)$, where

$$V(g_I) = H_*(CFK^-(g_I) \otimes_R \left(\bigotimes_{XX \in X(g_I)} R/(u^{(XX)}) \right)).$$

Theorem 4.10. *Let g be a special grid diagram for some possibly singular link L in $L(p, q)$. Assume at each crossing, g looks like the standard picture in **Figure 20**. Then there is a spectral sequence converging to $HFK^-(g)$ whose E_1 term is $V(g)$ with the differential d_1 induced by zip and unzip homomorphism.*

The proof of this theorem follows from the discussion in Section 4 of [25]. There are two important observations:

- (1) their existing proof relies only on the well-behaved diagram and chain complexes but not on the background manifold;

(2) as they mentioned in Section 6, when using a special grid diagram, all higher homotopies vanish. This has been seen during the proof of **Lemma 4.6**: Our Φ_A and Φ_B compose directly to multiplication by $-u^{(c)}$, with no need of the map Φ_{AB} in their terminology. This will also simplify higher differentials dramatically.

For each $c \in C(g)$, we denote by p_c , A_c and B_c the distinguished intersection point and mark points as shown in **Figure 22**. We say $\mathbf{x} \in \mathcal{S}(g)$ is

- of type Z_c if
 - c is positive and $p_c \in \mathbf{x}$;
 - c is negative and $p_c \notin \mathbf{x}$.
- of type Y_c if
 - c is positive and $p_c \notin \mathbf{x}$;
 - c is negative and $p_c \in \mathbf{x}$.

We say a rectangle r is

- of type A_c if
 - $r \in \text{Rect}^\circ(\mathbf{x}, \mathbf{y})$, one of \mathbf{x}, \mathbf{y} if of type Z_c , the other is of type Y_c ;
 - $n_{\mathbb{A}_c}(r) = 1$ and $n_{\mathbb{B}_c}(r) = 0$.
- of type B_c if
 - $r \in \text{Rect}^\circ(\mathbf{x}, \mathbf{y})$, one of \mathbf{x}, \mathbf{y} if of type Z_c , the other is of type Y_c ;
 - $n_{\mathbb{B}_c}(r) = 1$ and $n_{\mathbb{A}_c}(r) = 0$.
- of type AB_c if
 - $r \in \text{Rect}^\circ(\mathbf{x}, \mathbf{y})$, both \mathbf{x}, \mathbf{y} are of type Z_c ;
 - $n_{\mathbb{A}_c}(r) = 1$ and $n_{\mathbb{B}_c}(r) = 1$.

Let C_p denote the set of positive crossings g , C_n denote the set of negative ones. For disjoint set $I, J, K \subset C(g)$, let $Z_I = \cap_{c \in I} Z_c$, $Y_I = \cap_{c \in J} Y_c$, $Z_K = \cap_{c \in K} Z_c$.

Definition 4.11. Define $\Phi_{I,J,K} : Z_I \cap Y_J \cap Z_K \rightarrow Y_I \cap Z_J \cap Z_K$ by counting empty rectangles that are

- of type A_c for $c \in (I \cap C_p) \cup (J \cap C_n)$;
- of type B_c for $c \in (I \cap C_n) \cup (J \cap C_p)$;
- of type AB_c for $c \in K$;
- multiplicities at all other X or XX base points are zero.

Remark 4.12. From items in **Definition 4.2**, it follows immediately that $\Phi_{I,J,K}$ is zero whenever $K \neq \emptyset$ or $|I \cup J| > 1$. When $I = J = K = \emptyset$, $\Phi_{I,J,K}$ is just the usual differential.

Thus, in our case, Lemma 4.5 of [25] holds without need to prove.

Lemma 4.13. (Lemma 4.5 of [25]) Fix I, J, K disjoint as above, Then

$$\Sigma_{\{I_1, I_2, J_1, J_2, K_1, K_2 \mid I_1 \sqcup I_2 \sqcup K_1 \sqcup K_2 = I \cup K, J_1 \sqcup J_2 \sqcup K_1 \sqcup K_2 = J \cup K\}} \Phi_{I_1, J_1, K_1} \circ \Phi_{I_2, J_2, K_2} = \begin{cases} -u^{(c)}, & \text{if } K = \{c\} \text{ and } I = J = \emptyset \\ 0, & \text{otherwise} \end{cases}.$$

Now consider the graded group

$$C = \bigoplus_{I \sqcup J \sqcup K \sqcup L = C(g)} Z_I \cap Y_J \cap Z_K \cap Z_L,$$

the sum ranges over all partitions of $C(g)$ into disjoint subsets. Define a relation on the set of partitions by

$$(I_1, J_1, K_1, L_1) < (I_2, J_2, K_2, L_2),$$

if $I_2 \subset I_1$, $J_2 \subset J_1 \cup I_1$, $K_2 \subset I_1 \cup K_1$ and $|K_1 \Delta K_2| \leq 1$.

Definition 4.14. For such a pair of partitions, define a map

$$D_{(I_1, J_1, K_1, L_1) < (I_2, J_2, K_2, L_2)} : Z_{I_1} \cap Y_{J_1} \cap Z_{K_1} \cap Z_{L_1} \rightarrow Z_{I_2} \cap Y_{J_2} \cap Z_{K_2} \cap Z_{L_2}$$

$$\begin{cases} \Phi_{I_1 \cap J_2, L_2 \cap J_1, L_2 \cap I_1}, & \text{if } K_1 = K_2; \\ 1, & \text{if } K_2 = K_1 \cup \{n\}, J_1 = J_2, L_2 = L_1, n \text{ is a negative crossing}; \\ u^{(n)}, & \text{if } K_2 = K_1 - \{n\}, J_1 = J_2, I_1 = I_2, n \text{ is a negative crossing}; \\ u^{(p)}, & \text{if } K_2 = K_1 \cup \{p\}, J_1 = J_2, L_2 = L_1, p \text{ is a positive crossing}; \\ 1, & \text{if } K_2 = K_1 - \{p\}, J_1 = J_2, I_1 = I_2, p \text{ is a positive crossing}. \end{cases}$$

Endow C with the endomorphism

$$D = \sum_{(I_1, J_1, K_1, L_1) < (I_2, J_2, K_2, L_2)} D_{(I_1, J_1, K_1, L_1) < (I_2, J_2, K_2, L_2)}.$$

Lemma 4.15. (Lemma 4.6 of [25]) (C, D) is a chain complex quasi-isomorphic to $CFK^-(g)$.

Proof. The fact that $D^2 = 0$ follows immediately from **Remark 4.12** and **Lemma 4.13**. For each (I_1, J_1, K_1, L_1) , we consider the (I_2, J_2, K_2, L_2) component of $D^2|_{(I_1, J_1, K_1, L_1)}$. When $K_1 = K_2$, we have a square exactly the same as in **Equation 15**, so **Lemma 4.13** leads to the desired result. When $|K_1 \Delta K_2| = 1$ or 2 , we have a square with same map on the left and right hand side, and also same map on the top and bottom edges, since we are working over $\mathbb{F} = \mathbb{Z}/2\mathbb{Z}$, the result follows.

The quasi-isomorphism can be seen by a sub-quotient argument. In C , there is a subcomplex with trivial homology formed by those partitions with some positive crossings in K or L . The resulting quotient has a subcomplex consisting of those partitions with each negative crossing in $J \cup L$. This subcomplex can be identified with $CFK^-(g)$ while the resulting quotient has trivial homology. The identification can be done as follows: This sub-quotient complex has representative components of C with all positive crossings in $I \cup J$ and all negative crossings in $J \cup L$. In all these partitions $K = \emptyset$, so each generator in $\mathcal{S}(g)$ appears exactly once in it. For the identification of differential, it follows from **Remark 4.12** that $\Phi_{I, J, K}$ go back to differential when all of the three sets are empty, and the observation

- when $I = \{p\}$ consists of single crossing, a rectangle from $\mathbf{x} \in Z_p$ to $\mathbf{y} \in Y_p$ must contain one of B_p instead of A_p ;
- while when $J = \{n\}$ consists of single crossing, a rectangle from $\mathbf{x} \in Y_p$ to $\mathbf{y} \in Z_p$ must contain one of B_p instead of A_p .

These together show that all the nonzero components of D come from $\partial_{CFK^-(g)}^-$. Thus, we have proved our claim. \square

Proof. (of **Theorem 4.10**) (C, D) is actually a “partition-filtered” description of the $|C(g)|$ -dimensional resolution cube with all complete resolutions of $C(g)$ as an index set. Collapsing all vertical filtrations, we result in

$$\bigoplus_{I:C(g)\rightarrow\{0,1\}} CFK^-(g_I) \otimes_R \left(\bigotimes_{XX\in X(g_I)} R/(u^{(XX)}) \right),$$

with \mathcal{U}_c and \mathcal{Z}_c as edge homomorphisms. This and the quasi-isomorphism provided by **Lemma 4.15** give rise to the wanted spectral sequence. \square

5. AN ORIENTED VERSION

This section aims at extending the base ring of our grid homology from $\mathbb{Z}/2\mathbb{Z}$ to \mathbb{Z} . Our construction follows Chapter 15 of [26], Section 3 of [6] and Section 7 of [30]. Oriented resolution cube using braid diagram has also been used in [8] and [4]. The strategy will be assigning a sign to each rectangle embedded in the grid diagram, then considering the sign twisted differential and homology.

5.1. Sign assignment. Fix a grid diagram g for some link $L \subset L(p, q)$. For any pair of $\mathbf{x}, \mathbf{y} \in \mathcal{S}(g)$, we can consider the set $Rect(\mathbf{x}, \mathbf{y})$ of rectangles from \mathbf{x} to \mathbf{y} , which is either empty or consists of two elements. Ranging over all such pairs, we form a union

$$Rect(g) = \bigcup_{\mathbf{x}, \mathbf{y} \in \mathcal{S}(g)} Rect(\mathbf{x}, \mathbf{y}).$$

This will be the domain of our sign assignment.

Definition 5.1. *On a grid diagram g , a sign assignment is a function*

$$\mathbf{S} : Rect(g) \rightarrow \{\pm 1\}$$

satisfies

- (1) *If (r_1, r_2) and (r'_1, r'_2) form an alternative pair, i.e. $r_1 \in Rect(\mathbf{x}, \mathbf{w})$, $r_2 \in Rect(\mathbf{w}, \mathbf{z})$, $r'_1 \in Rect(\mathbf{x}, \mathbf{y})$, $r'_2 \in Rect(\mathbf{y}, \mathbf{z})$ with $\mathbf{y} \neq \mathbf{w}$ and $r_1 * r_2 = r'_1 * r'_2$, then $\mathbf{S}(r_1)\mathbf{S}(r_2) = -\mathbf{S}(r'_1)\mathbf{S}(r'_2)$;*
- (2) *If $r_1 * r_2$ is a horizontal annulus, then $\mathbf{S}(r_1)\mathbf{S}(r_2) = 1$;*
- (3) *If $r_1 * r_2$ is a vertical annulus, then $\mathbf{S}(r_1)\mathbf{S}(r_2) = -1$.*

In [6], they constructed sign assignments for grid diagrams of links in lens space using Spin central extension of the symmetric group (Following [11] and [26]) and fact that the set of generators $\mathcal{S}(g)$ can be identified with $S_n \times \mathbb{Z}/p\mathbb{Z}$ in a natural way.

By definition, a sign assignment on a grid diagram has nothing to do with the choices of O,X base points, so the existence and uniqueness shown in [6] extend directly to our case. Moreover, when fixing a grid diagram g , an explicit way of constructing an isomorphism between chain complexes

with different sign assignments is also given in [6], which is again base point-independent, so we have the following:

Theorem 5.2. (Theorem 1.1 of [6]) *Sign assignment exists for any grid diagram representing a possibly singular link L in $L(p, q)$ (actually unique up to certain kinds of gauge transformation). Moreover, for a fixed grid diagram, the sign-refined grid homology is independent of the choice of a sign assignment.*

With a chosen sign assignment \mathbf{S} on g , we now upgrade our chain group by replacing \mathbb{F} with \mathbb{Z} in **Definition 3.1** and redefining the differential to be

$$\partial_{\mathbf{S}}^- \mathbf{x} = \sum_{\mathbf{y} \in \mathcal{S}} \sum_{\{r \in \text{Rect}^\circ(\mathbf{x}, \mathbf{y}) \mid n_{\mathbb{X}}(r) = 0\}} \mathbf{S}(r) \prod_{i=1}^{2n+k} U_i^{n_{O_i}(r)} \mathbf{y};$$

$$\tilde{\partial}_{\mathbf{S}} \mathbf{x} = \sum_{\mathbf{y} \in \mathcal{S}} \sum_{\{r \in \text{Rect}^\circ(\mathbf{x}, \mathbf{y}) \mid n_{\mathbb{X}}(r) = 0, n_{\mathbb{O}}(r) = 0\}} \mathbf{S}(r) \mathbf{y}.$$

Using axioms in **Definition 5.1** one sees directly that

$$(\partial_{\mathbf{S}}^-)^2 = 0 \text{ and } (\tilde{\partial}_{\mathbf{S}})^2 = 0.$$

Indeed, when $\mathbf{x} \neq \mathbf{z}$, we have seen that each domain in $\pi(\mathbf{x}, \mathbf{z})$ has either zero or two ways to decompose into empty rectangles, and property (1) of \mathbf{S} shows that when there are two ways, they cancel with each other. When $\mathbf{x} = \mathbf{z}$, only annuli connect \mathbf{x} to itself. But these do not contribute to the differential since there is an X or XX base point in each horizontal or vertical annulus.

Now, we have shown that there are well-defined homology theories $HFK^-(g; \mathbb{Z})$ together with its two counterparts. Using the remark in **Theorem 5.2**, we shall omit the sign assignment from our notation.

5.2. Invariance of oriented theory. Discussion in the previous section shows that oriented homology theories are well-defined for each individual grid diagram. The aim of this section is to modify the proof in **Subsection 3.5** to show that these oriented theories won't change under grid moves, thus $HFK^\circ(L; \mathbb{Z})$ are well-defined link invariants.

Invariance of oriented theory for regular links in S^3 and lens spaces has been verified in [26] and [30], respectively. Note that the appearance of XX singular points only affects the grading of maps but has no influence on identities appeared in the proof to hold. We have proved in **Subsection 3.5** that gradings in our case behave correctly during grid moves. So it is straight forward to adapt their proof to our situation.

The basic idea behind their proof is to replace the various tools used in the proof with corresponding signed version. The main tasks in the following are

- relating sign assignments on different grid diagrams;
- defining signed version of all chain maps used in the proof.

5.2.1. Commutation invariance revisited. To adapt the previous proof of commutation invariance to the newly signed version, it is necessary to extend the definition of \mathbf{S} to pentagons and hexagons. Recall that we have relative grading formulas given by counting base points in rectangles:

$$M(\mathbf{x}, \mathbf{y}) = 1 + 2n_{\mathbb{X}\mathbb{X}}(r) - 2n_{\mathbb{O}}(r) + n_{\mathbf{x}}(\text{int}(r)) + n_{\mathbf{y}}(\text{int}(r)),$$

$$A(\mathbf{x}, \mathbf{y}) = 2n_{\mathbb{X}\mathbb{X}}(r) + n_{\mathbb{X}_r}(r) - n_{\mathbb{O}}(r).$$

On a grid diagram, the $Spin^c$ class of a generator is characterized by \mathbf{x} and \mathbf{y} belong to the same class if and only if they can be connected by a sequence of rectangles. Then the formula above implies that we can lift the Maslov grading in each $Spin^c$ class to a function $M_{\mathfrak{s}} : \mathcal{S}_{\mathfrak{s}} \rightarrow \mathbb{Z}$, here we use $\mathcal{S}_{\mathfrak{s}}$ to denote the set of generators in the $Spin^c$ structure \mathfrak{s} . This allows us to use $M(\mathbf{x})$ as exponent to control the sign. This is also necessary because examples computed in [30] show that the absolute grading which is canonical in the sense that can be identified with classical Heegaard Floer homology in the case of regular links is not integral valued in general.

Unfortunately, in [30], they directly used $M(\mathbf{x})$ defined in **Equation 6** as exponent of (-1) to characterize signs of pentagons which is a little weird. However, since the only property needed in their proof is when initial states of two pentagons are connected by a rectangle without X mark and of the same side (See the definition of \mathcal{S}_{Pent} below), then there is a sign (-1) appears in \mathcal{S} . So things get settled when we fix an integral lift of M for each $Spin^c$ class. We still denote by M the integral lift chosen class by class.

Assume g and g' are as described in **Subsubsection 3.5.1**, since a sign assignment has nothing to do with markings, we may fix a \mathcal{S} that works for both diagrams.

Recall that we have a closest point map $\mathbf{x} \mapsto \mathbf{x}'$ which is a bijection $\mathcal{S}(g) \rightarrow \mathcal{S}(g')$, and on the combined diagram we have a canonical small triangle $t_{\mathbf{x}}$ connecting each pair $(\mathbf{x}, \mathbf{x}')$. (See **Figure 17**.) When $p \in Pent(\mathbf{x}, \mathbf{y}')$, we have $t_{\mathbf{x}} * p \in Rect^{\circ}(\mathbf{x}', \mathbf{y}')$. Let $R(p)$ denote the rectangle associated to p in this way. A pentagon is said to be left (resp. right) if it lies to the left (resp. right) of the intersection point a on $\beta_i \cap \gamma_i$. Further, let $Pent(g, g')$ be the set of all pentagons from a generator in $\mathcal{S}(g)$ to some generator in $\mathcal{S}(g')$ in the combined diagram. With all these terminologies in hand, we define

$$\mathcal{S}_{Pent} : Pent(g, g') \rightarrow \{\pm 1\},$$

for $p \in Pent(\mathbf{x}, \mathbf{y}')$

$$\mathcal{S}_{Pent}(p) = \begin{cases} (-1)^{M(\mathbf{x})+1} \mathcal{S}(R(p)), & \text{if } p \text{ is a left pentagon;} \\ (-1)^{M(\mathbf{x})} \mathcal{S}(R(p)), & \text{if } p \text{ is a right pentagon.} \end{cases}$$

Recall that Maslov grading on $\mathcal{S}(g)$ and $\mathcal{S}(g')$ are identified so the fixed lift works for both. We can introduce sign assignment $\mathcal{S}_{Pent} : Pent(g', g) \rightarrow \{\pm 1\}$ in exactly the same way. In what follows, we shall omit the subscript ‘‘Pent’’.

Now we renew the pentagon counting maps to

$$P_{\mathcal{S}}(\mathbf{x}) = \sum_{\mathbf{y}' \in \mathcal{S}(g')} \sum_{\{p \in Pent^{\circ}(\mathbf{x}, \mathbf{y}') \mid p \cap \mathbb{X} = \emptyset\}} \mathcal{S}(p) \prod_{i=1}^{2n+k} U_i^{n_{O_i}(p)} \mathbf{y}'.$$

$$P'_{\mathcal{S}}(\mathbf{x}') = \sum_{\mathbf{y} \in \mathcal{S}(g)} \sum_{\{p \in Pent^{\circ}(\mathbf{x}', \mathbf{y}) \mid p \cap \mathbb{X} = \emptyset\}} \mathcal{S}(p) \prod_{i=1}^{2n+k} U_i^{n_{O_i}(p)} \mathbf{y}.$$

Lemma 7.2 in [30] shows that they are both chain maps using definition of \mathcal{S} .

Next, we further extend \mathcal{S} to $Hex(g)$, the set of all hexagon connecting generators in $\mathcal{S}(g)$ on the combined grid diagram. Recall that each $h \in Hex^{\circ}(\mathbf{x}, \mathbf{y})$ has $h * B \in Rect^{\circ}(\mathbf{x}, \mathbf{y})$, where B is one of the bigons shown in **Figure 17**. Define $R(h) = h * B$ and $\mathcal{S}(h) = \mathcal{S}(R(h))$. Renew H to

$$H_{\mathcal{S}}(\mathbf{x}) = \sum_{\mathbf{y} \in \mathcal{S}(g)} \sum_{\{h \in Hex^{\circ}(\mathbf{x}, \mathbf{y}) \mid h \cap \mathbb{X} = \emptyset\}} \mathcal{S}(h) \prod_{i=1}^{2n+k} U_i^{n_{O_i}(h)} \mathbf{y}.$$

Now Lemma 7.5 in [30] as well as Lemma 15.3.4 in [26] show that

$$\partial^- \circ H_{\mathbf{S}} + H_{\mathbf{S}} \circ \partial^- + P'_{\mathbf{S}} \circ P_{\mathbf{S}} + id_{CFK^-(g;\mathbb{Z})} = 0,$$

that is $P_{\mathbf{S}}$ and $-P'_{\mathbf{S}}$ are homotopy inverses to each other.

With the help of this, we know that $CFK^-(g;\mathbb{Z})$ and $CFK^-(g';\mathbb{Z})$ are quasi-isomorphic, which is exactly what we want.

5.2.2. Stabilization invariance revisit. Let g and g' be the pair considered in **Subsubsection 3.5.2**. Recall that all the maps used there count rectangles in g' , so things become transparent when we relate signs in g with those in g' . This can be done using $e : \mathbf{I} \rightarrow CFK^-(g)[U_{new}][1, 1]$ which is defined via bijection not only on the set of generators but also on the set of empty rectangles. Via this correspondence, a sign assignment $\mathbf{S} : Rect(g')$ gives rise to one on $Rect(g)$. Using this fact, a lift $M_{\mathbf{S}}$ for each $Spin^c$ class of generators on g' gives rise to one for g as well.

Using the chosen \mathbf{S} , we can enhance each of $H_{O_{new}}, H_{X_{new}}, H_{X_{new}, O_{new}}$ by adding $\mathbf{S}(r)$ to each term in the sum.

As noted in Section 15.3.2 of [26], still we have a square

$$\begin{array}{ccc} (\mathbf{I}^-, \partial_{\mathbf{I}}^{\mathbf{I}}) & \xrightarrow{\partial_{\mathbf{I}}^{\mathbf{N}}} & (\mathbf{N}^-, \partial_{\mathbf{N}}^{\mathbf{N}}) \\ \downarrow e & & \downarrow e \circ H_{X_{new}} \\ (CFK^-(g)[U_{new}][1, 1], -\partial_g^-) & \xrightarrow{U_{new} - U_j} & (CFK^-(g)[U_{new}][1, 1], \partial_g^-) \end{array}$$

Over \mathbb{Z} it is no longer commutative. Instead, each edge map anti-commutes with the differentials, and maps going right-down and down-right sum up to zero. Alternatively, consider the map $stab : CFK^-(g';\mathbb{Z}) \rightarrow Cone(U_{new} - U_j)$ defined by

$$stab(\mathbf{x}) = \begin{cases} (-1)^{M(\mathbf{x})} e(\mathbf{x}), & \mathbf{x} \in \mathbf{I} \\ (-1)^{M(\mathbf{x})} e \circ H_{X_{new}}(\mathbf{x}), & \mathbf{x} \in \mathbf{N} \end{cases},$$

on the set of generators and extends linearly to the whole complex. The property above can be reinterpreted as $stab$ being a chain map. This follows from (1) of **Definition 5.1**.

Again using (1)(2)(3) of **Definition 5.1**, one sees that

- **Proposition 3.6** still holds over \mathbb{Z} , so the choice of U_j on the same thin edge or S^1 component as U_{new} is still irrelevant.
- $H_{X_{new}} \circ H_{O_{new}} + Id_{\mathbf{I}^-} = 0$.
- $H_{O_{new}} \circ H_{X_{new}} + \partial_{\mathbf{N}}^{\mathbf{N}} \circ H_{X_{new}, O_{new}} + H_{X_{new}, O_{new}} \circ \partial_{\mathbf{N}^-}^{\mathbf{N}} + Id_{\mathbf{N}^-} = 0$

Note that two vertical maps are quasi-isomorphisms of chain complexes thanks to the identities above. Now the argument about mapping cone in **Subsubsection 3.5.2** and Lemma 5.2.12 in [26] finish the proof.

5.3. Oriented resolution cube. In this subsection, we are aiming to extend results in **Section 4** to an oriented version. Note that the resolution cube constructed in [25] and [16] are both over $\mathbb{F} = \mathbb{Z}/2\mathbb{Z}$, but some indication of signed convention appeared in an arxiv version of [25]. Recently,

oriented resolution cubes for knots in S^3 appeared in [4] and [8]. We now try their methods in our situation.

As in **Subsection 4.4**, we fix a special grid diagram g for some link L in $L(p, q)$ with standard picture as in **Figure 20** at each crossing. We assume the size of g is $n + k$ as usual, where n is the number of XX base points while k is the number of X base points. All the notations below will be same as in **Section 4**. By assumption on g , we have for each $c \in C(g)$, diagrams of $g_{c,s}$ and $g_{c,r}$ obtained from local modification. For a given complete resolution I , do as in **Figure 19** at each crossing, we obtain a compatible diagram g_I .

As we did when proving the invariance of oriented theory, once we choose a sign assignment for g , it gives rise to ones on the diagrams $g_{c,s}$ and $g_{c,r}$ for any $c \in C(g)$ as well as one on g_I for any complete resolution of g . Since in a standard picture we only modify the picture locally at each crossing, it suffices to show the existence of induced sign assignment on $g_{c,s}$ and $g_{c,r}$ for an arbitrary $c \in C(g)$. Recall that $g_{c,r}$ is obtained from g by changing the position of a pair of X base points, in particular, they share the same grid. Using the fact that a sign assignment has nothing to do with the set of O,X base point, one on g naturally gives rise to one on $g_{c,r}$. On the other hand, $g_{c,s}$ has grid states and rectangles in canonical one-to-one correspondence with a subcomplex of $CFK^-(g)$ (or $CFK^-(g_{c,r})$, depending on the sign of c) (See the proof of **Lemma 4.5**). So there is a unique sign assignment on $g_{c,s}$ compatible with the given one on g .

As in previous section, we fix an integral lift of Maslov grading in each $Spin^c$ structure on the diagram g . This gives rise to a lift of M for generators on all $g_{c,r}$, $g_{c,s}$, as well as g_I 's.

With these preparations in hand, we can now upgrade maps and complexes in **Section 4** to their counterparts over \mathbb{Z} . Since we used Q from the proof of **Lemma 4.5** to induce the sign assignment on $g_{c,s}$, it is now an isomorphism of chain complex over $\mathbb{Z}[U_1, \dots, U_{2n+k}]$. Now redefine maps $\Phi_A : Y \rightarrow Z$ and $\Phi_B : Z \rightarrow Y$ by

$$\Phi_A(\mathbf{x}) = \sum_{\mathbf{y} \in \mathcal{P}} \Sigma_{\{r \in \text{Rect}^\circ(\mathbf{x}, \mathbf{y}) \mid n_{\mathbb{X}_0}(r)=0, n_{\mathbb{A}}(r)=1\}} \mathbf{S}(r) \prod_{O_i \in \mathbb{O}} U_i^{n_{O_i}(r)} \mathbf{y};$$

$$\Phi_B(\mathbf{x}) = \sum_{\mathbf{y} \in \mathcal{C}} \Sigma_{\{r \in \text{Rect}^\circ(\mathbf{x}, \mathbf{y}) \mid n_{\mathbb{X}_0}(r)=0, n_{\mathbb{B}}(r)=1\}} \mathbf{S}(r) \prod_{O_i \in \mathbb{O}} U_i^{n_{O_i}(r)} \mathbf{y}.$$

These are still chain maps, which is guaranteed by (1) in the definition of \mathbf{S} .

In the proof of **Lemma 4.6**, we saw that only two thin horizontal annuli and two thin vertical annuli through the pairs of A_c , B_c base points contribute to $\Phi_A \circ \Phi_B$ and $\Phi_B \circ \Phi_A$. By (2)(3) in **Definition 5.1**, two horizontal annuli contribute multiplication by $U_c + U_d$, while vertical annuli contribute multiplication by $-U_a - U_b$. This shows that **Lemma 4.6** still holds, that is, $\Phi_A \circ \Phi_B$ and $\Phi_B \circ \Phi_A$ are both equal to multiplication by $U_c + U_d - U_a - U_b$.

From this, we can deduce that diagrams in **Equation 15** still commute. After obtaining these diagrams, proof of **Theorem 4.4** in **Subsection 4.2** is purely algebraic, so it now shows that the skein exact sequences in **Equation 13 and 14** still hold over \mathbb{Z} .

Now we move on to consider **Theorem 4.10**. Using diagrams in **Equation 15**, the zip and unzip homomorphisms can be defined as before. To prove the theorem, we construct a signed version of $\Phi_{I,J,K}$ and (C, D) . For $\Phi_{I,J,K}$, we only need to enhance the rectangle counting to an oriented version. Thanks to (1) of **Definition 5.1**, **Lemma 4.13** still holds. Together with the

sign conventions in (2)(3), one sees that $\Phi_A \circ \Phi_B$ and $\Phi_B \circ \Phi_A$ remain equal to multiplication by $-u^{(c)}$.

The group C is defined as in **Subsection 4.4** except each summand is now over the base ring \mathbb{Z} . **Definition 4.14** needs more care, we modify it as follows:

Definition 5.3. For any pair of partitions $(I_1, J_1, K_1, L_1) < (I_2, J_2, K_2, L_2)$, define a map

$$D_{(I_1, J_1, K_1, L_1) < (I_2, J_2, K_2, L_2), \mathbf{s}} : Z_{I_1} \cap Y_{J_1} \cap Z_{K_1} \cap Z_{L_1} \rightarrow Z_{I_2} \cap Y_{J_2} \cap Z_{K_2} \cap Z_{L_2}$$

$$\begin{cases} \Phi_{I_1 \cap J_2, L_2 \cap J_1, L_2 \cap I_1}, & \text{if } K_1 = K_2; \\ \pm 1, & \text{if } K_2 = K_1 \cup \{n\}, J_1 = J_2, L_2 = L_1, n \text{ is a negative crossing}; \\ \pm u^{(n)}, & \text{if } K_2 = K_1 - \{n\}, J_1 = J_2, I_1 = I_2, n \text{ is a negative crossing}; \\ \pm u^{(p)}, & \text{if } K_2 = K_1 \cup \{p\}, J_1 = J_2, L_2 = L_1, p \text{ is a positive crossing}; \\ \pm 1, & \text{if } K_2 = K_1 - \{p\}, J_1 = J_2, I_1 = I_2, p \text{ is a positive crossing}. \end{cases}$$

The sign depends on the Maslov grading of the generator \mathbf{x} as well as the crossing n or p . Fix an order $<$ on $C(g)$, then the sign is defined to be

$$(-1)^{M(\mathbf{x}) + |\{c \in K_1 \cap K_2 \mid c < n(c < p)\}|},$$

as they did in an arxiv version of [25] (See also [8]). Let $D_{\mathbf{S}}$ be the sum of these new maps, ranging over all such pairs. We now show that **Lemma 4.15** still holds.

To show that $D_{\mathbf{S}}^2 = 0$, we do as before: for each (I_1, J_1, K_1, L_1) , we consider the (I_2, J_2, K_2, L_2) component of $D^2|_{(I_1, J_1, K_1, L_1)}$. Assume the intermediate step is the summand corresponding to (I_3, J_3, K_3, L_3) . If the partitions (I_1, J_1, K_1, L_1) and (I_2, J_2, K_2, L_2) are identically the same, then things follows from $\partial^2 = 0$ using **Remark 4.12**. That remark also shows that for the map to be nonzero, at most two crossings change its belonging in I, J, K, L.

Next assume $K_1 = K_2$ but (I_1, J_1, K_1, L_1) and (I_2, J_2, K_2, L_2) are not identically the same. When $K_3 = K_2 = K_1$, again by **Remark 4.12**, for the maps to be nonzero, we can only have one crossing changing its position in I, J, K, L . We have two subcases to consider. In one case, we have a square with two groups on the left equal to (I_1, J_1, K_1, L_1) and the two on the right equal to $(I_2, J_2, K_2, L_2) = (I_1 - \{c\}, J_1 \cup \{c\}, K_1, L_1)$, whose contribution is

$$\partial \circ \Phi_{c, \emptyset, \emptyset} - \Phi_{c, \emptyset, \emptyset} \circ \partial = 0.$$

In the other case, we have $(I_3, J_3, K_3, L_3) = (I_1 - \{c\}, J_1 \cup \{c\}, K_1, L_1)$ and $(I_2, J_2, K_2, L_2) = (I_1 - \{c\}, J_1, K_1, L_1 \cup \{c\})$, so the composition is of form $\Phi_{\{c\}, \emptyset, \emptyset} \circ \Phi_{\emptyset, \{c\}, \emptyset}$ which is multiplication by $-u^{(c)}$ using **Lemma 4.6**, this will cancel with a component in which the intermediate group has $K_3 \neq K_1$. For intermediate groups with $K_3 \neq K_1$, it can only be $K_3 = K_1 \cup \{c\}$ using definition of the partial order (and in this case $c \in L_2$). Now the two maps must composite to $\pm u^{(c)}$. The sign is always $+$ since U multiplication has nothing to do with the parity of M and $K_1 \cap K_3 = K_3 \cap K_2$. For each such $K_3 \neq K_1$, there is exactly one partition $K'_3 = K_1$ such that from (I_1, J_1, K_1, L_1) , c first moves from I to J, then to L in (I_2, J_2, K_2, L_2) . This forms a square with the remaining case of $K_3 = K_1$, showing that $D^2 = 0$ when $K_1 = K_2$.

When $|K_1 \Delta K_2| = 1$, we show the case $K_2 = K_1 \cup \{n\}$ and $K_2 = K_1 - \{n\}$ as examples, positive case can be dealt with similarly. For the first one, the two possible intermediate steps are

$(I_1 - \{n\}, J_1, K_1 \cup \{n\}, L_1) = (I_2, J_2, K_2, L_2)$ or (I_1, J_1, K_1, L_1) for the maps to be nonzero. This leads to a square with two vertical maps all being ± 1 and two horizontal maps being restriction of ∂^- to $Z_I \cap Y_J \cap Z_K \cap Z_L$. The signed convention in **Definition 5.3** shows that it anti-commutes, that is $D_{\mathcal{S}}^2 = 0$. For the second one, the only two possible intermediate groups corresponding to partitions $(I_1, J_1, K_1 - \{n\}, L_1 \cup \{n\}) = (I_2, J_2, K_2, L_2)$ and (I_1, J_1, K_1, L_1) for the maps to be nonzero. The square will take the same form as in the first case (with vertical maps replaced by $\pm u^{(n)}$), showing that $D_{\mathcal{S}}^2 = 0$ in this case.

When $|K_1 \Delta K_2| = 2$, we must have one of the three cases: $K_2 = K_1 \cup \{c_1, c_2\}$, $K_2 = K_1 - \{c_1, c_2\}$ or $K_2 = (K_1 - \{c_1\}) \cup \{c_2\}$. In the first case, for the maps to be nonzero, the intermediate step can only belong to partitions $(I_1 - \{c_1\}, J_1, K_1 \cup \{c_1\}, L_1)$ or $(I_1 - \{c_2\}, J_1, K_1 \cup \{c_2\}, L_1)$. We again obtain a square with same maps up to sign on horizontal and vertical edges, both of the form $\pm u^{(c)}$ or 1 thus Maslov grading preserving. Note that exactly one of $c_1 < c_2$, $c_2 < c_1$ holds, without loss of generality assume the first. Then the composition with $(I_1 - \{c_1\}, J_1, K_1 \cup \{c_1\}, L_1)$ as an intermediate step has a negative sign, while the one goes through $(I_1 - \{c_2\}, J_1, K_1 \cup \{c_2\}, L_1)$ has a positive sign, showing that the square anti-commutes, thus sum to zero. This argument also applies to the remaining cases.

Combining all the discussion above, we can conclude that $D_{\mathcal{S}}^2 = 0$. The part of proof that $C \simeq CFK^-(g)$ is again purely algebraic, the added sign has no effect on the identification of D in the sub-quotient with ∂^- , so we have the desired quasi-isomorphism in oriented theory.

With all these lemmas prepared, we can prove **Theorem 4.10** as in **Subsection 4.4**.

Now we can conclude that skein relations and resolution cubes remain true for $HFK^-(L; \mathbb{Z})$.

REFERENCES

- [1] Benjamin Audoux. Singular link Floer homology. *Algebr. Geom. Topol.*, 9(1):495–535, 2009.
- [2] Kenneth L. Baker, J. Elisenda Grigsby, and Matthew Hedden. Grid diagrams for lens spaces and combinatorial knot Floer homology. *Int. Math. Res. Not. IMRN*, (10):Art. ID rnm024, 39, 2008.
- [3] Yuanyuan Bao. Floer homology and embedded bipartite graphs, 2018. arXiv:1401.6608.
- [4] Anna Beliakova, Krzysztof Karol Putyra, Louis-Hadrien Robert, and Emmanuel Wagner. A proof of dunfield-gukov-rasmussen conjecture. 2022.
- [5] Francis Bonahon. Difféotopies des espaces lenticulaires. *Topology*, 22(3):305–314, 1983.
- [6] Daniele Celoria. A note on grid homology in lens spaces: \mathbb{Z} coefficients and computations. *Glasgow Mathematical Journal*, 65(2):457–479, 2023.
- [7] Peter R. Cromwell. Embedding knots and links in an open book i: Basic properties. *Topology and its Applications*, 64(1):37–58, 1995.
- [8] Nathan Dowlin. A spectral sequence from Khovanov homology to knot Floer homology. *J. Amer. Math. Soc.*, 37(4):951–1010, 2024.
- [9] Ivan Dynnikov. Arc-presentations of links. monotonic simplification. *Fundamenta Mathematicae*, 190, 08 2002.
- [10] Boštjan Gabrovšek and Eva Horvat. Knot invariants in lens spaces. In Colin C. Adams, Cameron McA. Gordon, Vaughan F.R. Jones, Louis H. Kauffman, Sofia Lambropoulou, Kenneth C. Millett, Jozef H. Przytycki, Renzo Ricca, and Radmila Sazdanovic, editors, *Knots, Low-Dimensional Topology and Applications*, pages 347–361, Cham, 2019. Springer International Publishing.
- [11] Etienne Gallais. Sign refinement for combinatorial link floer homology. *Algebraic & Geometric Topology*, 8:1581–1592, 2007.
- [12] Shelly Harvey and Danielle O’Donnol. Heegaard Floer homology of spatial graphs. *Algebr. Geom. Topol.*, 17(3):1445–1525, 2017.
- [13] Louis H. Kauffman. Invariants of graphs in three-space. *Trans. Amer. Math. Soc.*, 311(2):697–710, 1989.

- [14] Akio Kawauchi. A survey of knot theory. 1996.
- [15] Robert Lipshitz. A cylindrical reformulation of Heegaard Floer homology. *Geom. Topol.*, 10:955–1096, 2006. [Paging previously given as 955–1097].
- [16] Ciprian Manolescu. An untwisted cube of resolutions for knot Floer homology. *Quantum Topol.*, 5(2):185–223, 2014.
- [17] Ciprian Manolescu, Peter Ozsváth, and Sucharit Sarkar. A combinatorial description of knot Floer homology. *Ann. of Math. (2)*, 169(2):633–660, 2009.
- [18] Ciprian Manolescu, Peter Ozsváth, Zoltán Szabó, and Dylan Thurston. On combinatorial link Floer homology. *Geom. Topol.*, 11:2339–2412, 2007.
- [19] Peter Ozsváth, András Stipsicz, and Zoltán Szabó. Floer homology and singular knots. *J. Topol.*, 2(2):380–404, 2009.
- [20] Peter Ozsváth and Zoltán Szabó. Absolutely graded Floer homologies and intersection forms for four-manifolds with boundary. *Adv. Math.*, 173(2):179–261, 2003.
- [21] Peter Ozsváth and Zoltán Szabó. Holomorphic disks and knot invariants. *Adv. Math.*, 186(1):58–116, 2004.
- [22] Peter Ozsváth and Zoltán Szabó. Holomorphic disks and three-manifold invariants: properties and applications. *Ann. of Math. (2)*, 159(3):1159–1245, 2004.
- [23] Peter Ozsváth and Zoltán Szabó. Holomorphic disks and topological invariants for closed three-manifolds. *Ann. of Math. (2)*, 159(3):1027–1158, 2004.
- [24] Peter Ozsváth and Zoltán Szabó. Holomorphic disks, link invariants and the multi-variable Alexander polynomial. *Algebr. Geom. Topol.*, 8(2):615–692, 2008.
- [25] Peter Ozsváth and Zoltán Szabó. A cube of resolutions for knot Floer homology. *J. Topol.*, 2(4):865–910, 2009.
- [26] Peter S. Ozsváth, András I. Stipsicz, and Zoltán Szabó. *Grid homology for knots and links*, volume 208 of *Mathematical Surveys and Monographs*. American Mathematical Society, Providence, RI, 2015.
- [27] V. V. Prasolov and A. B. Sossinsky. *Knots, links, braids and 3-manifolds*, volume 154 of *Translations of Mathematical Monographs*. American Mathematical Society, Providence, RI, 1997. An introduction to the new invariants in low-dimensional topology, Translated from the Russian manuscript by Sossinsky [Sosinskiĭ].
- [28] Jacob Andrew Rasmussen. *Floer homology and knot complements*. ProQuest LLC, Ann Arbor, MI, 2003. Thesis (Ph.D.)—Harvard University.
- [29] Sucharit Sarkar and Jiajun Wang. An algorithm for computing some heegaard floer homologies. *Annals of Mathematics*, 171(2):1213–1236, 2010.
- [30] Samuel Tripp. On grid homology for lens space links: combinatorial invariance and integral coefficients, 2021. arXiv:2110.00663.
- [31] Zipei Zhuang. Grid homology for spatial graphs and a skein exact sequence. 2021. arXiv:2109.13694.